AD-A173 369 NONLINEAR MULTIGRID FOR THE EULER EQUATIONS: THE ONE-DIMENSIONAL SCALAR C..(U) STANFORD UNIV CA CENTER FOR LARGE SCALE SCIENTIFIC COMPUTATIO.. W A MULDER 1/1

UNCLASSIFIED 09 JUL 86 CLASSIC-86-11 N00014-82-K-0335 F/G 9/2 NL

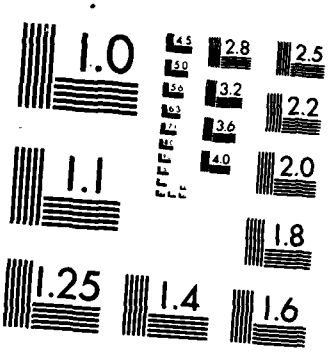

CLaSSiC Project
Manuscript CLaSSiC-86-11

July 1986

# Nonlinear Multigrid for the Euler Equations: The One–Dimensional Scalar Case

William A. Mulder



Center for Large Scale Scientific Computation
Building 460, Room 313
Stanford University
Stanford, California 94305

# Nonlinear multigrid for the Euler equations: the one-dimensional scalar case

William A. Mulder
Department of Computer Science
Stanford University
Stanford, CA 94305-2140

July 9, 1986

**Abstract.** A recent multigrid method for computing steady inviscid compressible flow is analyzed for the one-dimensional scalar case. The discretization in space by means of upwind differencing has first- or second-order accuracy. Three types of relaxation schemes that use only local information are examined. A numerical experiment with a smooth steady solution shows good agreement with the estimated damping rates. A discontinuous solution displays slower convergence. This is mainly caused by the singularity at the shock. The singularity can be removed by the additional constraint of local conservation, which is achieved through a special kind of local relaxation, using information about conservation from coarser grids. The sonic point causes some slow-down as well, but this can be neglected in practical applications. It turns out that a first-order-accurate solution can be obtained by 1 F-cycle per grid, whereas second-order accuracy requires about 4.

**Key words**: multigrid method, hyperbolic conservation laws, shock waves

## 1. Introduction

The multigrid technique is a powerful tool for the construction of $O(N)$ methods for a wide class of problems. Especially the solution of elliptic PDE's has received much attention, and the technique is well established for these problems [3,4,13]. It has taken some time before any results for hyperbolic equations, specifically the Euler equations of gas-dynamics, were obtained, but successful experiments are now available [6,7,10].

In [10] it was demonstrated that the $O(N)$ behaviour can indeed be obtained for the relatively simple problem of transonic flow through a channel with a circular bump on one wall. The multigrid technique used is essentially standard, thanks to discretization by means of upwind differencing. It is applied to a linear system based on the nonlinear equations. A direct nonlinear formulation, known as a Full Approximation Storage (FAS) scheme, is not fundamentally different from this approach. Indeed it was shown in [5] that the nonlinear version of the technique in [10], with minor variations, yields a similarly good performance. FAS is more expensive [7], but more versatile, especially when local grid-refinement is used.

A major drawback of the technique so far, is the necessity to use many multigrid cycles, as opposed to the one, or few, cycles that are usually sufficient for elliptic problems. An example can be found in [11]. There, however, an ill-posed problem was studied, and the solution was forced to convergence far below the truncation error (which could not be completely defined because of the ill-posedness). But even under better circumstances the multigrid technique does not seem to completely live up to the expectations [6,7,8].

This paper provides some insight in what can actually be expected, and what is the cause of failing expectations, by considering the simplest nonlinear model equation one can think of: the one-dimensional scalar inviscid Burgers' equation.

This work has been supported by the Center for Large Scale Scientific Computing (CLaSSiC) Project at Stanford under the Office of Naval Research Contract N00014-82-K-0335.

Both a smooth and a discontinuous test problem are considered (§2). The spatial discretization is obtained through upwind differencing by Roe's scheme [12], with first- or second-order accuracy.

In §3 three relaxation schemes are described that use only local information. This property is desirable for vectorization, parallelization, and local grid-refinement. Their smoothing rates are estimated from a linearized version of the nonlinear differential equation.

The multigrid scheme is described in §4. By combining the relaxation operator (§3.2) with the Coarse-Grid Correction (CGC) operator (§4.1), we can obtain the asymptotic convergence rates for various schemes (§4.2). Some ideal relaxation schemes, that have an estimated damping rate of zero in regions where the velocity is well above, or well below, zero, are considered in §4.3. The Full Multigrid scheme (FMG), with its restriction and prolongation operators, is described in §4.4.

The associated amount of work is estimated in §4.5. Solution errors and stopping criteria are reviewed in §4.6. The practical construction of a relaxation scheme is described in §4.7.

The analysis breaks down if the velocity of the flow changes its sign. At the shock, the discrete equations become singular. This is appropriate, because the original differential equations are singular. The singularity can be removed by augmenting the differential equations with the Rankine-Hugoniot jump relations, which are implicit in the conservation form of the equations. The time-accurate discrete equations in conservation form resolve the singularity in the same way. However, time-accuracy has been sacrificed here to obtain fast convergence. Thus, we need an alternative way to remove the singularity. This can be achieved by imposing local conservation through a special kind of local relaxation, using information about conservation from the coarser grids (§4.8).

At the sonic point, we analyze the damping rate in a different way, now using the linearized difference equations. Only Point-Jacobi for a first-order-accurate solution is considered here (§4.9).

Numerical results on the two test cases are presented in §5. A comparison between estimated and experimental asymptotic damping rates is made (§5.1). Next, the minimum number of cycles required to obtain a steady state within the truncation error is considered (§5.2). Two multigrid extensions, the deferred correction technique and $\tau$-extrapolation, are discussed in §5.3 and §5.4, respectively.

The main conclusions are summarized in §6.

## 2. Test Problems

We consider two types of steady solutions to the one-dimensional scalar hyperbolic equation

$$u_t + (\tfrac{1}{2}u^2)_x = s(x), \tag{2.1}$$

the first being smooth, the second discontinuous. These solutions are periodic in x on the interval $[0, 1)$. Setting

$$u(x) = c_0 + \sin 2\pi(x - \xi), \quad c_0 = 2, \tag{2.2a}$$

leads to a source term

$$s(x) = 2\pi \left(c_0 + \sin 2\pi(x - \xi)\right) \cos 2\pi(x - \xi). \tag{2.2b}$$

Although the steady state corresponding to this source term is continuous, a shock may occur during the evolution toward the steady state.

A discontinuous steady solution is found for

$$s(x) = \tfrac{1}{2}\pi \sin 2\pi(x - \xi), \tag{2.3a}$$

namely,

$$u(x) = \begin{cases} \sin \pi(x-\xi) & \text{for } 0 \le x < \xi + \frac{1}{2}, \\ -\sin \pi(x-\xi) & \text{for } \xi + \frac{1}{2} < x \le 1. \end{cases} \tag{2.3b}$$

For $0 < \xi < \frac{1}{2}$, this solution has a sonic point at $x = \xi$ and a shock at $x = \xi + \frac{1}{2}$ (cf. [15]). Numerical examples will be given for $\xi = 0.1$. In both cases the solution is periodic. It should be remarked that Eq.(2.1) must be interpreted as the limit for zero viscosity $\nu$ of the same equation with $\nu u_{xx}$ added to the right-hand side.

A computational grid with N zones is defined by $x_k = (k + \frac{1}{2})h$, where the cell-size $h = 1/N$ and $k = 0, \ldots, N-1$. Equation (2.1) is discretized in space by averaging per volume:

$$u_k = I^h u \equiv \frac{1}{h} \int_{x_k - \frac{1}{2}h}^{x_k + \frac{1}{2}h} dx\, u(x), \tag{2.4}$$

The same discretization operator $I^h$ is applied to the residual

$$r(u, x) = s(x) - (\tfrac{1}{2}u^2)_x, \tag{2.5}$$

yielding

$$r_k(u) = s_k - \frac{1}{h}(f_{k+\frac{1}{2}} - f_{k-\frac{1}{2}}). \tag{2.6}$$

The fluxes $f_{k \pm \frac{1}{2}}$ are evaluated by *upwind differencing*. Godunov's scheme lets

$$f_{k+\frac{1}{2}} = f(u_k, u_{k+1}) = \tfrac{1}{2} \max\big( \max(0, u_k)^2, \min(0, u_{k+1})^2 \big). \tag{2.7}$$

We use Roe's scheme [12,15], which in this case is identical to Godunov's scheme except for its treatment of the sonic point:

$$f_{k+\frac{1}{2}} = f(u_k, u_{k+1}) = \tfrac{1}{2} u_k u_{k+1}, \quad \text{if } u_k \le 0 \le u_{k+1}. \tag{2.8}$$

With this flux, the solution at the sonic point is smooth, whereas Godunov's scheme sets $f_{k+\frac{1}{2}} = 0$, causing an $O(h)$ jump.

The numerical steady solution $\overline{u}_k^h$ obeys $r_k(\overline{u}_{k-1}, \overline{u}_k, \overline{u}_{k+1}) = 0$ for $i = 0, \ldots, N-1$. It is first-order accurate, i.e., $\|\overline{u}_k^h - u_{ek}^h\| = O(h)$, where $u_{ek}^h \equiv I^h u(x)$ is the average per cell of the exact solution, and $\| \cdot \|$ is a relevant norm.

Second-order spatial accuracy can be obtained by assuming the solution to be piecewise linear rather than piecewise constant [15]. The idea is to write the solution as

$$u(x) = u_k + (\frac{x - x_k}{h})\Delta_k, \quad \frac{|x - x_k|}{h} < \tfrac{1}{2}. \tag{2.9}$$

Here $\Delta_k$ is related to the average derivative of the solution within cell k:

$$\Delta_k \equiv \int_{x_k - \frac{1}{2}h}^{x_k + \frac{1}{2}h} dx\, \frac{\partial u}{\partial x}. \tag{2.10}$$

Its numerical value can be computed from $u_{k-1}, u_k, u_{k+1}$ by

$$\Delta_k = ave(u_k - u_{k-1},\, u_{k+1} - u_k). \tag{2.11}$$

In smooth regions we want $ave(\Delta_-, \Delta_+) = \frac{1}{2}(\Delta_- + \Delta_+)$, whereas some limiting to the smaller of $\Delta_-$ and $\Delta_+$ is required near discontinuities to preserve monotonocity (i.e., to avoid local under- or overshoots). We use an averaging-limiting procedure from [1]:

$$ave(\Delta_-, \Delta_+) = \frac{(\Delta_+^2 + \epsilon_a^2)\Delta_- + (\Delta_-^2 + \epsilon_a^2)\Delta_+}{\Delta_-^2 + \Delta_+^2 + 2\epsilon_a^2}. \tag{2.12}$$

The bias $\epsilon_a$ prevents division by zero. Clipping of smooth extrema is avoided if $\epsilon_a$ approximately equals the average value of $|u_k - u_{k-1}|$ in smooth regions of the flow. For the numerical examples mentioned above we adopt $\epsilon_a = 4h$ for the smooth problem (2.2) and $\epsilon_a = 2h$ for the discontinuous problem (2.3). Once the $\Delta_k$ are computed, the fluxes $f_{k+\frac{1}{2}}$ are evaluated by $f(u_k + \frac{1}{2}\Delta_k, u_{k+1} - \frac{1}{2}\Delta_{k+1})$, using either Godunov's (2.7) scheme or Roe's scheme (2.7,2.8). It should be remarked that the scheme has second-order accuracy almost everywhere. In the worst case, there remains an $O(h)$ error in the cells near the shock. The rest of the solution has an $O(h^2)$ error.

Apart from the smoother behaviour of the first-order Roe scheme near the sonic point, there is another reason for preferring Roe's scheme above Godunov's, as will be seen in §4.7.

The numerical problem of determining the steady state to (2.1) can be written as

$$r_k(u_{k-p}, \ldots, u_{k+p}) = 0, \quad \text{for } k = 0, \ldots, N-1. \tag{2.13}$$

Here $p = 1$ for a first-order and $p = 2$ for a second-order scheme. For the example given in Eq.(2.3), (2.13) is ill-posed. Suppose that $u_L > 0$ is the state in the cell at the left from the shock, $u_R < 0$ at the right, and that $u_M$ is the state in the cell that contains the shock: $u_L > u_M > u_R$. Then the residual for the first-order scheme $r_M = s_M - (\frac{1}{2}u_R^2 - \frac{1}{2}u_L^2)$, which is independent of $u_M$. Thus, the state $u_M$ never enters the discrete equations (2.13) and can be chosen arbitrarily, as long as $u_L > u_M > u_R$. For a second-order scheme, $u_L$ and $u_R$ are replaced by $u_L + \frac{1}{2}\Delta_L$ and $u_R - \frac{1}{2}\Delta_R$ in the expression for the residual. The average differences $\Delta_L$ and $\Delta_R$ will depend on $u_M$, but if the latter state is not close to either $u_L$ or $u_R$, limiting will occur. In this way the $\Delta_L$ and $\Delta_R$ become small, and the residual behaves practically the same as in the first-order case. As a consequence, one expects the numerical non-uniqueness to persist in the second-order scheme, although $\overline{u}_M$ will be confined to a smaller interval than that for the first-order case.

The singular behaviour at the shock is the immediate consequence of dropping the time-dependency from the original equation. In a time-accurate integration, the conservation form of the equation automatically takes care of the jump equation across the discontinuity. Then

$$\frac{1}{N}\sum_{k=0}^{N-1} u_k = C \quad \text{(a constant)}, \tag{2.14}$$

for each time-step. In this way the singularity does not occur. If the integration is not time-accurate, the final $\overline{u}_M$ can be recovered from

$$\overline{u}_M = NC - \sum_{k=0, k\neq M}^{N-1} \overline{u}_k, \tag{2.15}$$

but only if there is *one* shock. Alternatively, the detailed structure in zone $k = M$ may be used to find $\overline{u}_M$ (see [15]). In this paper we will use *local conservation* as an additional constraint to remove the singularity. Conservation is imposed on the coarsest grid. On fine grids the information about conservation is obtained from the next coarser grid (§4.8).

## 3. Relaxation schemes

**3.1. Construction.** The problem of determining a steady solution to Eq.(2.13) can be written in a more abstract form by introducing a nonlinear operator

$$L(u) = (\tfrac{1}{2}u^2)_x \tag{3.1a}$$

and its discrete version

$$L_k^h(u^h) = \frac{1}{h}(f_{k+\frac{1}{2}} - f_{k-\frac{1}{2}}). \tag{3.1b}$$

The error $v^h \equiv \overline{u}^h - u^h$, where $\overline{u}^h$ is the steady state, obeys

$$L^h(u^h + v^h) - L^h(u^h) = r^h. \tag{3.2}$$

A relaxation scheme provides an approximate solution $\tilde{v}^h$ to Eq.(3.2). An example is the explicit scheme

$$\Big[\frac{1}{\Delta t}\Big]\Delta_t u^h = r^h, \quad \Delta_t u^h \equiv \tilde{u}^h - u^h, \tag{3.3}$$

or the implicit scheme

$$\Big[\frac{1}{\Delta t} - \alpha\Big(\frac{dr}{du}\Big)^h\Big]\Delta_t u^h = r^h. \tag{3.4}$$

Here $\alpha$ determines the amount of under- ($\alpha > 1$) or over-relaxation ($\alpha < 1$). The choice $\alpha = 1$ yields a "backward Euler" scheme. If the time-step $\Delta t$ becomes large, the latter reduces to Newton's method. This property is exploited by the Switch Evolution/Relaxation (SER) scheme, proposed in [9,16], where $\Delta t \propto 1/\|r^h\|$. After some initial time-dependent searching while the residuals are large, this scheme automatically switches to Newton's method when the solution approaches the steady state.

For a one-dimensional problem, Eq.(3.4) with a residual (2.13) of first-order accuracy ($p = 1$) requires the solution of a tridiagonal system. This system can be approximated by retaining only the unaltered main-diagonal. Alternatively, it can be replaced a diagonal system composed of the original main- and off-diagonals [16].

For the purpose of analysis we consider a linearized version of the original equation:

$$u_t + au_x = s(x). \tag{3.5}$$

Here $a$ is assumed to be positive, for the moment. Equation (3.2) reduces to

$$L^h v^h = r^h, \tag{3.6a}$$

and a relaxation scheme provides an approximate solution $\tilde{v}^h$ through

$$\tilde{L}^h \Delta_t v^h = L^h v^h, \quad \Delta_t v = \tilde{v}^h - v^h. \tag{3.6b}$$

Here it is assumed that the approximation $\tilde{L}^h$ to $L^h$ makes (3.6b) easy to solve. The last equation can be rewritten in terms of a relaxation operator

$$S^h = I - (\tilde{L}^h)^{-1} L^h, \tag{3.7a}$$

namely,

$$\tilde{v}^h = S^h v^h. \tag{3.7b}$$

Let the usual CFL-number be denoted by $\sigma \equiv \Delta t\,|a|/h$ and the shift operators by $Tu_k \equiv u_{k+1}$, $T^{-1}u_k \equiv u_{k-1}$. For positive $a$, we have

$$L^h = \frac{a}{h}(1 - T^{-1}). \tag{3.8}$$

The explicit scheme is given by

$$\tilde{L}^h = \frac{1}{\Delta t}, \tag{3.9}$$

whereas the implicit scheme lets

$$\tilde{L}^h = \Big[\frac{1}{\Delta t} - \alpha\Big(\frac{dr}{du}\Big)^h\Big] = \Big[\frac{1}{\Delta t} + \alpha L^h\Big], \tag{3.10}$$

a lower bidiagonal system. Replacing the translation operator by a scalar multiplication $\omega$ results in

$$\tilde{L}^h = \frac{1}{\Delta t}\Big[1 + \alpha\sigma(1-\omega)\Big], \tag{3.11}$$

a diagonal matrix. For the scalar one-dimensional problem studied here, the last expression results in the same relaxation operator as the one for an explicit scheme:

$$S^h = 1 - \beta(1 - T^{-1}), \tag{3.12}$$

where

$$\beta = \sigma, \tag{3.13a}$$

for an explicit scheme, and

$$\beta = \frac{\sigma}{1 + \alpha\sigma(1-\omega)} \tag{3.13b}$$

for the diagonal approximation (3.11) of the implicit scheme (3.4). The relaxation scheme (3.12) can be analyzed for different values of the parameter $\beta$. Although the explicit and diagonal approximation of the implicit scheme are equivalent, according to (3.12), their difference lies in the construction of a fixed value for $\beta$ (3.13). In the case of non-constant $a$, or for systems of equations, the implicit scheme provides more clues for this construction then the explicit one. We will leave this subject now, and assume that $\beta$ is merely an adjustable parameter of the relaxation scheme.

**3.2. Smoothing rates.** To analyze the stability and damping of the relaxation schemes, we write $v^h$ as a Fourier-series

$$v_k^h = \sum_{l=0}^{N-1} \hat{v}_l^h \exp\big(2\pi i \frac{kl}{N}\big), \quad k = 0, \ldots, N-1. \tag{3.14}$$

Let the Fourier operator $F^h$ and its inverse $(F^h)^{-1}$ have elements

$$F_{lk}^h = \frac{1}{N}\exp\big(-2\pi i\frac{kl}{N}\big), \quad (F^h)_{kl}^{-1} = \exp\big(2\pi i\frac{kl}{N}\big), \tag{3.15}$$

then

$$\hat{v}^h = F^h v^h, \quad v^h = (F^h)^{-1}\,\hat{v}^h. \tag{3.16}$$

The relaxation operator in the Fourier domain becomes

$$\hat{S}^h = F^h S^h\,(F^h)^{-1}. \tag{3.17}$$

The scheme is stable if the spectral radius $\rho(\hat{S}^h) \leq 1$. The symbol of the translation operator $T$ is

$$\hat{T} = \exp(i\theta), \quad \theta \equiv 2\pi l/N. \tag{3.18}$$

For practical purposes $\theta$ may be assumed to be a continuous quantity ($N \to \infty$). The damping of the scheme can be analyzed by evaluating the amplification factor $\mu(\theta) \equiv \hat{S}^h(\theta)$.

A multigrid method requires a relaxation scheme that has good smoothing for short waves. We will now consider three relaxation schemes based on (3.12), which can be easily generalized to systems in one or more dimensions, use only local information, and can be vectorized.

The first relaxation scheme to be considered is Point-Jacobi relaxation (PJ). All cells in the computational domain are updated independently. The corresponding growth-factor is given by

$$\mu(\theta) = 1 - \beta(1 - \hat{T}^{-1}). \tag{3.19}$$

Stability requires

$$|\mu(\theta)|^2 = 1 - 2\beta(1-\beta)(1-\cos\theta) \leq 1, \quad \theta \in [-\pi, \pi], \tag{3.20a}$$

implying

$$0 \leq \beta \leq 1. \tag{3.20b}$$

Choosing $\beta = 0$ does not make sense, of course.

For a *single-grid* scheme, the choice $\beta = 1$ has some special properties. The growth-factor is $\mu(\theta) = \hat{T}^{-1}$ in that case. The explicit scheme runs at the maximum local time-step. For an implicit scheme, a step with $\beta = 1$ can be interpreted as a Point-Jacobi iteration for Newton's method [PJ implies $\omega = 0$, i.e., the off-diagonals are neglected; Newton's method is obtained for $\alpha = 1$ and a very large time-step $\Delta t$, i.e., $\sigma \to \infty$]. In a physical interpretation, the local errors can be viewed as waves. For $\beta = 1$ these are convected over a distance $h$, the cell-size. For a problem with boundaries, or with shocks, we thus expect a single-grid scheme with $\beta = 1$ to yield fastest convergence. Errors (in the sense of deviations from the numerical steady state) are convected as fast as possible toward the boundaries, where they leave the computational domain, or toward a shock, where they are absorbed by the dissipation in the shock. Because $|\mu(\theta)| = 1$, there is no damping in smooth regions of the flow, which is consistent with the differential equation. Conservation in time and time-accuracy, however, are lost. The latter is not very important for steady-state computations, as long as the correct final steady state is found. (For complicated problems, a SER scheme may be safer [16].) If conservation in time is necessary for the uniqueness of the final solution, it can be imposed as a global condition at the end of one or more relaxation sweeps. For a periodic shockless problem, as in (2), the differential equation has no mechanism to get rid of the initial errors, and a steady state can formally never be reached. In practice, the discretization error in the numerical flux provides a small amount of dissipation that damps the error. The relaxation scheme can provide additional dissipation. For PJ, the maximum amount of dissipation is obtained if $\beta = \frac{1}{2}$.

The second relaxation scheme is a Multi-Stage scheme (MS). Here we consider only 2 stages. The first stage is a PJ step with $\beta = \beta_1$, advancing the solution $u$ to $u'$. The second stage is again PJ relaxation, but with $\beta = \beta_2$. Now the solution $u$ is advanced to $\tilde{u}$, using the residual $r' = r(u')$. The growth-factor for one MS step is

$$\mu(\theta) = 1 - \beta_2(1 - \hat{T}^{-1})[1 - \beta_1(1 - \hat{T}^{-1})], \tag{3.21a}$$

which is stable for

$$|\beta_1| \leq \frac{1}{2}, \quad 0 \leq \beta_2 \leq 1 + 2\beta_1. \tag{3.21b}$$

At the stability limit $\beta_1 = \frac{1}{2}$, $\beta_2 = 2$, and $\mu = \hat{T}^{-2}$.

The third relaxation scheme considered in this paper, is checkerboard or Red-Black relaxation (RB). It consists of a PJ sweep on the even points ($k = 0, 2, \ldots, N-2$), an update of the solution and residuals, followed by a similar operation on the odd points ($k = 1, 3, \ldots, N-1$):

$$\left.\begin{aligned} \tilde{v}_{2k} &= (1-\beta)v_{2k} + \beta v_{2k-1} \\ \tilde{v}_{2k+1} &= (1-\beta)v_{2k+1} + \beta \tilde{v}_{2k} \end{aligned}\right\} \quad k = 0, 1, \ldots, \tfrac{1}{2}N - 1. \tag{3.22}$$

In the Fourier domain

$$\tilde{\hat{v}}_l = \left[1-\beta(1-\hat{T}^{-1}) - \tfrac{1}{2}\beta^2\hat{T}^{-1}(1-\hat{T}^{-1})\right]\hat{v}_l - \tfrac{1}{2}\beta^2\hat{T}^{-1}(1+\hat{T}^{-1})\hat{v}_{l+N/2}, \quad l = 0, 1, \ldots, N-1. \tag{3.23}$$

This implies that the Fourier components at $l$ and $l+N/2$ are coupled. If the elements $(l, l+N/2)$ are grouped, then

$$\begin{pmatrix} \tilde{\hat{v}}_l \\ \tilde{\hat{v}}_{l+N/2} \end{pmatrix} = \hat{S}^h \begin{pmatrix} \hat{v}_l \\ \hat{v}_{l+N/2} \end{pmatrix}, \quad \hat{S}^h \equiv \begin{pmatrix} \hat{s}_{11} & \hat{s}_{12} \\ \hat{s}_{21} & \hat{s}_{22} \end{pmatrix}, \quad l = 0, \ldots, \tfrac{1}{2}N - 1, \tag{3.24a}$$

where

$$\begin{aligned} \hat{s}_{11}(\hat{T}) &= 1 - \beta(1-\hat{T}^{-1}) - \hat{s}_{12}(-\hat{T}), \\ \hat{s}_{12}(\hat{T}) &= -\tfrac{1}{2}\beta^2\hat{T}^{-1}(1+\hat{T}^{-1}), \end{aligned} \tag{3.24b}$$

and

$$\begin{aligned} \hat{s}_{21}(\hat{T}) &= \hat{s}_{12}(-\hat{T}), \\ \hat{s}_{22}(\hat{T}) &= \hat{s}_{11}(-\hat{T}). \end{aligned} \tag{3.24c}$$

Here we have used the fact that

$$\hat{T}_{l+N/2} = -\hat{T}_l, \quad \hat{T}_l \equiv \hat{T} = \exp(2\pi i l/N). \tag{3.25}$$

Because of this, the expressions for $\hat{s}_{21}$ and $\hat{s}_{22}$ are immediately recovered from $\hat{s}_{11}$ and $\hat{s}_{12}$. The product of two matrices with property (3.24c) again has this property.

The eigenvalues of $\hat{S}$ are

$$\lambda_\pm = \tfrac{1}{2}(\hat{s}_{11} + \hat{s}_{22}) \pm \tfrac{1}{2}[(\hat{s}_{11} - \hat{s}_{22})^2 + 4\hat{s}_{12}\hat{s}_{21}]^{\frac{1}{2}}, \tag{3.26}$$

Because the $v_k$ are real, we have $|\hat{v}_l| = |\hat{v}_{N-l}|$, so only the values $l = 0, 1, \ldots, \frac{1}{2}N$ or $\theta \in [0, \pi]$ have to be considered. Furthermore, if the $\hat{v}_l$ are grouped according to $(l, l+N/2)$, it is sufficient to consider $l = 0, 1, \ldots, N/4$ or $\theta \in [0, \pi/2]$, because $|\hat{v}_{l+N/2}| = |\hat{v}_{N/2-l}|$. If $\hat{S}$ is diagonal, then, for a given $\theta \in [0, \pi/2]$, the modulus of $\lambda_- = \hat{s}_{11}(\theta)$ describes the amplification of the long waves ($\theta \in [0, \pi/2]$), whereas the modulus of $\lambda_+ = \hat{s}_{22}(\theta) = \hat{s}_{11}(\pi - \theta)$ describes the growth of the short waves. If $\hat{S}$ is not diagonal, the eigenvalues can no longer be assigned to these parts of the spectrum.

Following [3], the best relaxation schemes in a multigrid context are those for which

$$\overline{\mu} = \max_{\theta \in [\frac{1}{2}\pi, \pi]} |\mu(\theta)| \tag{3.27}$$

is as small as possible. Here it is assumed that $\hat{S}$ is diagonal. For non-diagonal $\hat{S}$, [3] *defines*

$$\overline{\mu} \equiv \max_{\theta \in [0, \pi/2]} |\hat{s}_{22}(\theta)| = \max_{\theta' \in [\pi/2, \pi]} |\hat{s}_{11}(\theta')|. \tag{3.28}$$

The parameter $\beta$, or the pair $(\beta_1, \beta_2)$, can be tuned to minimize $\overline{\mu}$. Table 1 lists the optimum choices. The optimum $\beta$ for RB is the root of $\beta^3 + \beta = 1$. However, for a purely convective

equation, these choices may not lead to fastest MG convergence, as will be seen in the next section. The main point is the *diffusion* of the schemes with minimum $\overline{\mu}$. It will be shown that *smoothing* the error is sufficient. For RB, this can be done without damping.

We continue with the smoothing rates for second-order schemes. The differential operator for the linear case, in a smooth region of the flow, is

$$L^h = \frac{a}{h}(1-\hat{T}^{-1})(1+\tfrac{1}{4}(\hat{T}-\hat{T}^{-1})). \tag{3.29}$$

The Point-Jacobi scheme has a growth-factor

$$\mu = 1-\beta(1-\hat{T}^{-1})(1+\tfrac{1}{4}(\hat{T}-\hat{T}^{-1})). \tag{3.30}$$

There is no value $\beta \neq 0$ for which this scheme is stable.

The MS scheme with second-order spatial accuracy is stable for $0 \leq \beta_1 \leq \frac{1}{2}, 0 \leq \beta_2 \leq 2\beta_1$. The smallest value for $\overline{\mu}$ is obtained for $\beta_1 = \frac{1}{2}(1+3\sqrt{5})$, $\beta_2 = \frac{2}{55}(23-3\sqrt{5})$.

Finally, second-order Red-Black relaxation is stable for $0 \leq \beta \leq 1$. The smallest value of $\overline{\mu}$ is obtained for the root of $45\beta^3 + 4\beta = 8$. A variation of Red-Black relaxation is obtained if the linear distribution characterized by $\Delta_k$ is frozen during relaxation. This scheme, however, can not be stabilized for any $\beta \neq 0$ (contrary to the remark in [16]).

The values of $\beta$ for which $\overline{\mu}$ is smallest are listed is Table 1.

## 4. Multigrid relaxation

**4.1. Coarse-grid correction operator.** The convergence speed of a relaxation scheme can be improved by the use of coarser grids. The communication between grids is controlled by restriction and prolongation operators. Here we use the same operators as in [10]. Restriction brings the averages of pairs of cells to a coarser grid, whereas prolongation brings coarse-grid information back to the fine grid. In this section we will analyze the behaviour of the multigrid scheme by two-level analysis (cf. [3]). It is assumed that the equations on the next coarser grid (having $N/2$ cells) are solved exactly.

The two-level amplification operator is

$$M = (S^h)^{\nu_2}[I - I_H^h (L^H)^{-1} I_h^H L^h](S^h)^{\nu_1}. \tag{4.1}$$

It describes the result of applying the relaxation operator $S^h$ for $\nu_1$ steps, restrict the residuals on grid h to the coarse grid H by the restriction operator $I_h^H$, solve the coarse-grid problem exactly, prolongate the coarse-grid correction to the fine grid by $I_H^h$, add this correction to the fine-grid solution, and, finally, perform $\nu_2$ additional relaxation sweeps. We will now derive an explicit expression the coarse-grid correction (CGC) operator

$$K = [I - I_H^h (L^H)^{-1} I_h^H L^h]. \tag{4.2}$$

given our specific problem.

The restriction operator $I_h^{2h}$ lets

$$r_k^{2h} = \tfrac{1}{2}(r_{2k}^h + r_{2k+1}^h), \quad k = 0, 1, \ldots, \tfrac{1}{2}N. \tag{4.3}$$

Here the choice $H = 2h$ has been made. Note that the definition of $I_h^{2h}$ is consistent with the definition of the discretization operator $I^h$ in (2.4), and preserves the conservation form of the residual (2.6). The prolongation operator is $I_{2h}^h = I$: the coarse-grid correction $\tilde{v}^H$ is simply distributed over the fine grid.

With the above restriction operator, the coarse-grid residual becomes

$$r_k^{2h} = \left(I_h^{2h} L^h v^h\right)_k = \frac{a}{2h}(T - T^{-1})v_{2k}, \quad k = 0, 1, \ldots, \tfrac{1}{2}N - 1. \tag{4.4}$$

In the Fourier domain

$$\hat{r}_l^{2h} = \frac{a}{2h}(\hat{T} - \hat{T}^{-1})(\hat{v}_l^h - \hat{v}_{l+N/2}^h), \quad l = 0, 1, \ldots, \tfrac{1}{2}N - 1. \tag{4.5}$$

The result is 0 for the shortest and longest wave. For the shortest wave $\hat{T} = -1$ and the restriction operator $\hat{I}_h^{2h}$ makes this one invisible on the coarse grid. The longest wave with $\hat{T} = 1$ is already made invisible on the fine grid by the residual operator $\hat{L}^h$. We thus have

$$\hat{K}(\theta) = 1, \quad \text{for } \theta = 0, \pi. \tag{4.6}$$

The coarse grid operator $L^{2h} = \frac{a}{2h}(1 - \hat{T}^{-2})$, so in the physical domain the CGC operator $K$ lets

$$\left.\begin{aligned} \tilde{v}_{2k} &= v_{2k} - v_{2k+1} \\ \tilde{v}_{2k+1} &= 0 \end{aligned}\right\} \quad k = 0, 1, \ldots, \tfrac{1}{2}N - 1. \tag{4.7}$$

Here the longest and shortest waves have been ignored. In Fourier space, the exact solution of the coarse-grid equation yields

$$\hat{v}_l^{2h} = \begin{cases} \hat{T}(\hat{v}_l^h - \hat{v}_{l+N/2}^h), & l = 1, \ldots, \tfrac{1}{2}N - 1, \\ 0, & l = 0, \tfrac{1}{2}N. \end{cases} \tag{4.8}$$

The prolongation operator $\hat{I}_{2h}^h$ lets

$$\tilde{\hat{v}}_l^h = \hat{v}_l^h - \tfrac{1}{2}(1 + \hat{T}^{-1})\hat{v}_l^{2h}, \quad l = 0, 1, \ldots, N - 1. \tag{4.9}$$

Note that $\hat{v}_l^{2h}$ has a period $N/2$, whereas $\hat{v}_l^h$ has a period $N$ in $l$. For the symbol $\hat{K}$ of the CGC operator, the elements $(l, l + N/2)$ or $(\theta, \theta + \pi)$ can again be grouped in pairs, as in (3.24a), yielding

$$\hat{k}_{11} = \tfrac{1}{2}(1 - \hat{T}), \quad \hat{k}_{12} = \tfrac{1}{2}(1 + \hat{T}), \quad \hat{T} = \exp(i\theta), \quad \theta \in (0, \pi/2]. \tag{4.10a}$$

The elements $\hat{k}_{21}$ and $\hat{k}_{22}$ are found through property (3.24c).

Equation (4.6) states that the coarse-grid correction has no effect on the shortest and the longest waves. The shortest wave can be taken care of by the relaxation operator $S^h$. The longest wave represents a constant value. If, as in practical computations, a *sequence* of coarser grids is used instead of only one, this constant value can be introduced on the coarsest grid as a global constraint. In our examples, we use a coarsest grid of 2 cells, with values $u_0^{h_1}$ and $u_1^{h_1}$, which should obey (2.14). The constant $C = c_0$ for example (2.2); $C = 0$ for example (2.3). The actual values $u_0^{h_1}$ and $u_1^{h_1}$ are determined as the exact solution on the grid with cell-size $h_1$, which obeys (2.13) and (2.14). In this way, we effectively have $\hat{K} = 0$ for $\theta = 0$, or, more precisely,

$$\hat{K} = \begin{pmatrix} 0 & 0 \\ 0 & 1 \end{pmatrix}, \quad \text{for } (l, l + N/2) = (0, N/2) \text{ or } (\theta, \pi - \theta) = (0, \pi). \tag{4.10b}$$

Apart from this, the two-level analysis provides a reasonable approximation to the amplification matrix of a many-level multigrid correction, because the use of multigrid relaxation for the problem on the grid with cell-size $2h$ usually provides a very good solution.

For a second-order scheme we find the following expression

$$\begin{aligned} \hat{k}_{11} &= 1 - \tfrac{1}{2}(1+\hat{T})\tfrac{1+\frac{1}{4}(\hat{T}-\hat{T}^{-1})}{1+\frac{1}{4}(\hat{T}^2-\hat{T}^{-2})}, \\ \hat{k}_{12} &= \quad \tfrac{1}{2}(1+\hat{T})\tfrac{1-\frac{1}{4}(\hat{T}-\hat{T}^{-1})}{1+\frac{1}{4}(\hat{T}^2-\hat{T}^{-2})}, \\ \hat{T} &= \exp(i\theta), \quad \theta \in (0, \pi/2]. \end{aligned} \tag{4.11}$$

For $\theta = 0$ we again have (4.10b). Alternatively, we may consider a second-order-accurate discretization on the fine grid, and a first-order discretization on the coarse grid. Then

$$\begin{aligned} \hat{k}_{11} &= 1 - \tfrac{1}{2}(1+\hat{T})\left(1+\tfrac{1}{4}(\hat{T}-\hat{T}^{-1})\right), \\ \hat{k}_{12} &= \quad \tfrac{1}{2}(1+\hat{T})\left(1-\tfrac{1}{4}(\hat{T}-\hat{T}^{-1})\right). \end{aligned} \tag{4.12}$$

For $\theta = 0$ we should use (4.10b).

**4.2. Asymptotic convergence rates.** The quality of a relaxation scheme in combination with the CGC operator can be characterized by

$$\overline{\lambda} = \max_{\theta \in [0,\pi/2]} \rho(\hat{M}). \tag{4.13}$$

Here $\hat{M}$ is again ordered in the pairs $(\theta, \pi - \theta)$, so that the maximum is effectively taken over the entire spectrum. The value of $\overline{\lambda}$ will depend only on $\nu = \nu_1 + \nu_2$, for a given relaxation scheme [13]. We will now re-evaluate the three relaxation schemes in this context.

Consider the PJ scheme. The smallest value of $\overline{\lambda}$ is obtained for $\beta = \frac{1}{2}$. In that case we have, for $\nu = 1$ and $p = 1$,

$$\hat{K}^h \hat{S}^h = -\tfrac{1}{4}(\hat{T} - \hat{T}^{-1}) \begin{pmatrix} 1 & -1 \\ 1 & -1 \end{pmatrix}. \tag{4.14}$$

The spectral radius $\overline{\lambda}$=0. Table 2a shows the values of $\overline{\lambda}$ for various $\beta$. For a second-order scheme, PJ is unstable for long waves, but the coarse-grid correction stabilizes these waves. This scheme can not be called robust, but one may get away with the instability in practical applications. For a first-order-accurate discretization, the choice $\beta = \frac{1}{2}$ and $\nu = 1$ is clearly the best. For second-order accuracy, the first-order CGC yields the best results. It does not pay to choose $\nu = 2$, because the improvement of the damping rate does not compensate the additional work involved, as compared to $\nu = 1$.

The results for the Multi-Stage scheme, with two stages, are listed in Table 2b. For a first-order-accurate discretization, one better uses a PJ scheme. For second-order accuracy, a second-order CGC ($p = 2$) and $\nu = 1$ is the best choice in terms of the amount of work involved.

The third relaxation scheme to be considered is Red-Black. Here there is a pitfall. So far, the convection speed $a$ has been assumed to be positive. In the cases considered above, the final results are the same for negative $a$. With RB relaxation, the asymmetry in the relaxation scheme interacts with the asymmetry in the CGC operator, thus producing different results for positive and negative convection speeds. Instead of $a > 0$ and $a < 0$, we can just as well consider the effect of the *order* in which RB is carried out. So far, we have used the order $(even, odd)$ for a grid with cells $k = 0, 1, \ldots, N-1$. The final results for $a < 0$ and the order $(even, odd)$ are the same as those for $a > 0$ and the order $(odd, even)$. Table 2c lists the results for both the order $(even, odd)$ and $(odd, even)$, assuming $a > 0$. Note that $\overline{\mu}(\nu = 2) \neq [\overline{\mu}(\nu = 1)]^2$, in contrast to the two previous relaxation schemes.

The first-order scheme with $\beta = 1$ produces a matrix $\hat{K}^h\hat{S}^h \equiv 0$, but only with the order $(even, odd)$ and $a > 0$. We can obtain $\hat{K}^h\hat{S}^h = 0$ for positive and negative convection speeds, if the order of the RB scheme is adapted to the direction of the convection on the coarser grid. If the average convection speed in the pair of zones $(2k, 2k+1)$, $k = 0, 1, \ldots, \frac{1}{2}N-1$, is positive, first the even and then the odd cells are relaxed, whereas for a negative convection speed the order $(odd, even)$ is used. We propose to name this scheme *Convective Red-Black* (CRB) relaxation. This scheme is *ideal* when used with a first-order-accurate discretization, because the combination with the CGC operator vanishes.

**4.3. Ideal relaxation schemes.** RB relaxation is known to be order-free. This property is lost when RB is embedded in our multigrid scheme. CRB effectively is a marching scheme in the multigrid context, like Gauss-Seidel (c.f. [10,16]). The obvious reason for this behaviour is the structure of $K$ and $\hat{K}$ in Eqs. (4.7) and (4.10), respectively. Given these expressions, the problem of designing a good relaxation scheme can be approached from the opposite direction: which scheme, when used in combination with (4.7) or (4.10), gives the smallest value of $\overline{\lambda}$ for a given amount of work?

An *ideal* relaxation scheme obviously should have the property

$$v_{2k} = v_{2k+1}, \quad \text{for } k = 0, 1, \ldots, \tfrac{1}{2}N - 1. \tag{4.15}$$

This means that the remaining error can be represented, and consequently be solved exactly, on the coarse grid. CRB, with $\beta = 1$ has this property. A more economic scheme is obtained if relaxation is carried on half the number of cells. Such a scheme may be called *Red* or *Black*, but the name *Semi Red-Black* is probably less confusing. There are several variants: we can relax only the even points, or only the odd, or take the direction of the flow into account. Assume $a > 0$. Then the order $(even, odd)$ results in a relaxation operator, that, for $\beta = 1$, is given by

$$\hat{S}_f = \tfrac{1}{2}\begin{pmatrix} 1+\hat{T}^{-1} & -1-\hat{T}^{-1} \\ -1+\hat{T}^{-1} & 1-\hat{T}^{-1} \end{pmatrix}. \tag{4.16}$$

The subscript $f$ stands for forward relaxation, in the same direction as the flow. The backward variant, corresponding to the order $(even, odd)$, is

$$\hat{S}_b = \tfrac{1}{2}\begin{pmatrix} 1+\hat{T}^{-1} & 1+\hat{T}^{-1} \\ 1-\hat{T}^{-1} & 1-\hat{T}^{-1} \end{pmatrix}, \tag{4.17}$$

again for $\beta = 1$. The product of either relaxation operator with the first-order CGC operator $\hat{K}$ has an eigenvalue $\overline{\lambda} = 0$. However, for one combination we have the stronger result that the product vanishes, namely:

$$\hat{K}\hat{S}_b \equiv 0. \tag{4.18a}$$

The effect of $\hat{S}_b$ is equivalent with (4.15). Furthermore,

$$\hat{S}_f\hat{K} = 0 \quad \text{for } \hat{T} \neq 1, \quad \hat{S}_f\hat{K} = \begin{pmatrix} 0 & -1 \\ 0 & 0 \end{pmatrix} \quad \text{for } \hat{T} = 1. \tag{4.18b}$$

If the longest waves ($\hat{T} = 1$) are ignored, the CGC operator $\hat{K}$ causes the error to obey (4.7), i.e., the odd cells have an error $v^h_{2k+1} = 0$. Applying $\hat{S}_f$ on the even cells makes the error in cell $2k$ equal to the error in cell $2k-1$ by convection, resulting in a zero error everywhere. For $\nu_1 = \nu_2 = 1$ we have $S_fKS_f \equiv 0$, $S_fKS_b \equiv 0$, and $S_bKS_b \equiv 0$. However, $S_bKS_f$ has $\overline{\lambda} = 2$ and is useless.

The convective variant of SRB is denoted by CSRB. We choose the combination (4.18a) if $(\nu_1, \nu_2) = (1, 0)$, and (4.18b) if $(\nu_1, \nu_2) = (0, 1)$. If both $a > 0$ and $a < 0$ occur, the operators $S_f$ and $S_b$ are different from the expressions in (4.16) and (4.17), but still are directed along with, or against the flow. For instance, $S_f$ on the pairs $(2k, 2k+1)$, $k = 0, 1, \ldots, \frac{1}{2}N - 1$, updates the even cells if the average value of the convection speed $\frac{1}{2}(a_k + a_{k+1})$ is positive, and the odd if this average speed is negative. The operator $S_b$ does the opposite.

For second-order spatial accuracy, there is no obvious relaxation scheme that removes the error completely in combination with the CGC step.

It should be noted that optimizing $\overline{\mu}$, as suggested in [3], does not necessarily give the optimal value of $\overline{\lambda}$.

**4.4. Full Multigrid.** The performance of these relaxation schemes has been tested as part of a Full Multigrid Scheme (cf. [3]). We start on a grid $m = 1$ with 2 cells, having a cell-size $h_1$, were the solution is computed directly from the nonlinear discrete equations, using the conservation condition (2.14) as an additional constraint. On the finer grids $m = 2, 3, \ldots$, with $N = 2^m$, we obtain an initial guess of the solution by interpolation of the coarser solution $(m-1)$ to the actual fine grid $m$. The corresponding operator will be denoted by $I_h^H$. Then a number of nonlinear multigrid or FAS (Full Approximation Storage) cycles are carried out to find the steady state within truncation order.

The interpolation of the final solution on grid $m-1$ to grid $m$ requires an order of accuracy consistent with the solution. We first describe the interpolation of a second-order-accurate solution. In smooth regions of the flow, the solution on grid $m-1$ is assumed to be piecewise parabolic:

$$u_k^H(x) = u_k^H + \xi \Delta_k^{(1)} + \tfrac{1}{2}(\xi^2 - \tfrac{1}{12})\Delta_k^{(2)}, \quad \xi \equiv \tfrac{x - x_k}{H}. \tag{4.19}$$

Here $\Delta_k^{(1)}$ equals the earlier $\Delta_k$ of Eq. (2.10), whereas $\Delta_k^{(2)}$ is a discrete approximation to

$$\Delta_k^{(2)} \equiv \int_{x_k - \frac{1}{2}h}^{x_k + \frac{1}{2}h} dx \, \frac{\partial^2 u}{\partial x^2}. \tag{4.20}$$

The interpolation to the grid with cell-size $h = H/2$ is done by

$$u^h = I_H^h(u^H): \quad \begin{cases} u_{2k}^h \;\; = \dfrac{1}{h} \displaystyle\int_{x_k^H - h}^{x_k^H} dx \; u_k^H(x) = u_k^H - \tfrac{1}{4}\Delta_k^{(1)}, \\ u_{2k+1}^h = \dfrac{1}{h} \displaystyle\int_{x_k^H}^{x_k^H + h} dx \; u_k^H(x) = u_k^H + \tfrac{1}{4}\Delta_k^{(1)}, \end{cases} \tag{4.21}$$

Here the second-order term drops out. In the first-order case the same result is obtained. In practice $\Delta_k^{(1)}$ on the coarser grid with cell-size $H$ is computed by means of the same averaging-limiting procedure as before (2.12).

For completeness we present our restriction and prolongation operator again. Restriction involves the computation of

$$\left.\begin{aligned} u_k^H &= \tfrac{1}{2}(u_{2k}^h + u_{2k+1}^h), \\ r_k^H &= \tfrac{1}{2}(r_{2k}^h + r_{2k+1}^h), \\ \tau_{h,k}^H &= r_k^H - r(u_k^H). \end{aligned}\right\} \quad k = 0, 1, \ldots, \tfrac{1}{2}N - 1. \tag{4.22}$$

The coarse-grid problem now becomes

$$r_k^H(u^H) + \tau_{h,k}^H = 0, \quad \text{or} \quad L_k^H(u^H) = s_k^H + \tau_{h,k}^H. \tag{4.23}$$

The approximate solution $\tilde{u}_k^H$ of this coarse-grid problem is prolongated back to the fine grid by

$$\begin{aligned} \tilde{u}_{2k}^h &= u_{2k}^h + (\tilde{u}_k^H - \tfrac{1}{2}(u_{2k}^h + u_{2k+1}^h)) = \tfrac{1}{2}(u_{2k}^h - u_{2k+1}^h) + \tilde{u}_k^H, \\ \tilde{u}_{2k+1}^h &= u_{2k+1}^h + (\tilde{u}_k^H - \tfrac{1}{2}(u_{2k}^h + u_{2k+1}^h)) = \tfrac{1}{2}(u_{2k+1}^h - u_{2k}^h) + \tilde{u}_k^H. \end{aligned} \tag{4.24}$$

In the actual computer program, we have multiplied $s_k^h$ and $r_k^h$ by $h$, which simplifies the restriction of the residual somewhat, and is generally recommended for non-uniform grids (cf. [11]).

The multigrid strategy is specified by $\nu_1$, $\nu_2$, and $\gamma$. Here $\nu_1$ denotes the number of sweeps before restriction, $\nu_2$ after prolongation, whereas $\gamma$ is the number of multigrid cycles on the coarser grid $H$ before returning to $h$. A flow-chart for this strategy can be found in [13, pg. 45]. For $\gamma = 1$ we have a V-cycle, for $\gamma = 2$ a W-cycle. A less expensive version of the latter is the F-cycle [3], also with $\gamma = 2$. Here the first cycle from grid $H$ is a W-cycle, the second a V-cycle, and so on for all coarser grids.

**4.5. Work.** The amount of work $w'$ involved in one multigrid correction cycle on grid $m$ with $2^m$ cells is given by

$$w' = A_m(\gamma)\,[\nu w_x + w_r + w_p] + B_m(\gamma) w_e. \tag{4.25a}$$

Here $w_x$ is the amount of work required for a relaxation sweep, $w_r$ for restriction, and $w_p$ for prolongation. The cost of the exact solution on grid $m = 1$ with $N = 2$ cells is expressed by $w_e$. The constants $A_m(\gamma)$ and $B_m(\gamma)$ depend on the total number of grids $m$ and the type of strategy:

$$A_m(\gamma) = \sum_{n=0}^{m-2} (\gamma/2)^n, \quad B_m(\gamma) = \frac{1}{2}(\gamma/2)^{m-2}. \tag{4.25b}$$

Both $A_m(\gamma)$ and $B_m(\gamma)$ are zero for $m < 2$. For $w_e$ this implies that the cost of the exact inversion is only counted during the multigrid correction cycle. For large $m$, we have $A_m(1) \simeq 2$, yielding a total amount of work proportional to $N$. A W-cycle has $A_m(2) = m - 1 = \log_2(N/2)$. For $\gamma > 2$ and large $m$, we have $A_m(\gamma) \propto N^{\log_2 \gamma}$. An F-cycle has $\gamma = 2$, but still results in an $O(N)$ algorithm. It has:

$$A_m^F = \sum_{n=0}^{m-2} (n+1)(\frac{1}{2})^n, \quad B_m^F = (m-1)(\frac{1}{2})^{m-1}. \tag{4.25c}$$

For large $m$, $A_m^F \simeq 4$, which is twice the cost of a V-cycle.

In our case, the evaluation of the residual is the most time-consuming part of the algorithm. If we set $w_x = 1$ for the PJ scheme, then $w_x = 2$ for MS. For RB we also have $w_x = 2$, but in other cases we may obtain $w_x = 1$ (for instance, if first-order flux-vector splitting for a system of equations is used; cf. [9,10,11,16]). Restriction requires the computation of the fine-to-coarse defect correction, which involves the computation of the residual on the fine and the next coarser grid. The coarse-grid residual can be used for the relaxation scheme or further restriction, so we only have to count the fine-grid work, implying $w_r \simeq 1$. One may exploit the special structure of the residual to lower $w_r$, but this has not been done in this paper. The cost of prolongation ($w_p$) is neglected. The first time the exact inversion on the grid with $N = 2$ cells is carried out, the discrete source term $s_k$ can be used directly and no residual has to be computed. In this case $w_e$ is neglected, as already mentioned above. During the multigrid correction cycle, we need $\tau_{h,k}^H$ on the coarsest grid, implying that the residual has to be computed. In that case we let $w_e = 1$.

The total amount of work required to obtain a solution on grid $M$ using the FMG-scheme is given by

$$w_M = \kappa[C_M(\gamma)(\nu w_x + w_r + w_p) + D_M(\gamma)w_e], \tag{4.26a}$$

Here $\kappa$ denotes the number of multigrid correction cycles used to find the steady state on each grid. The constants $C_M(\gamma)$ and $D_M(\gamma)$ depend on the strategy used:

$$C_M(\gamma) = \sum_{m=2}^{M} A_m(\gamma)2^{m-M}, \quad D_M(\gamma) = \sum_{m=2}^{M} B_m(\gamma)2^{m-M}. \tag{4.26b}$$

For V-, W-, and F-cycles, this results in

$$\begin{aligned} C_M(1) &= 4 - (\tfrac{1}{2})^{M-2}(M+1), & D_M(1) &= (\tfrac{1}{2})^{M-1}(M-1); \\ C_M(2) &= 2(M-2) + (\tfrac{1}{2})^{M-2}, & D_M(2) &= 1 - (\tfrac{1}{2})^{M-1}; \\ C_M^F &= 8 - (\tfrac{1}{2})^{M-1}(M^2+3M+4), & D_M^F &= M(M-1)(\tfrac{1}{2})^M. \end{aligned} \tag{4.26c}$$

**4.6. Solution error and stopping criteria.** There are several ways to determine whether or not the solution on a given finest grid has converged. A simple approach is to compute the number of cycles required for convergence below the discretization error from the estimated $\overline{\lambda}$, and hope for the best. In this case the initial residual, after in interpolation of the stationary solution on the coarser grid, should be brought down by a factor $(\frac{1}{2})^{1+p}$.

An adaptive approach involves a comparison between the residuals and an estimate of the discretization error. The latter is defined by

$$\tau_k^h \equiv L_k^h\big(I^h(\overline{u})\big) - I_k^h\big(L(\overline{u})\big) = -r_k(\overline{u}_e^h). \tag{4.27}$$

Here $\overline{u}$ is the exact stationary solution of the differential equation, and $\overline{u}_e^h = I^h(\overline{u})$. The operator $I^h$ is given by Eq.(2.4). Note that the steady solution $\overline{u}^h$ of the discrete problem, obeying $r_k(\overline{u}^h) = 0$, differs form $\overline{u}_e^h$ by $O(h^p)$. The corresponding error in the stationary solution

$$E^h \equiv \overline{u}^h - \overline{u}_e^h. \tag{4.28}$$

Following [3], the discretization error in the residual $\tau^h$ can be estimated by assuming $\tau^h(x) \simeq c(x)h^p$, where $c(x)$ is independent of $h$. Then

$$\tau^{2h}(x) \simeq \frac{1}{1-(\frac{1}{2})^p}\tau_h^{2h}(x), \quad \tau_h^{2h} = \tau^{2h} - \tau^h. \tag{4.29a}$$

From this expression we can estimate

$$\tau^h(x) \simeq (\tfrac{1}{2})^p I_{2h}^h(\tau^{2h}). \tag{4.29b}$$

The fine-to-coarse correction $\tau_h^{2h}$ is computed during restriction (4.22). Although Eq.(4.29a) should contain the $\tau_h^{2h}$ computed from steady solutions on grid $h$ and $2h$, the actual value during the multigrid cycling can be used as an estimate.

If one does not want to use the non-steady estimate for $\tau_h^{2h}$, $\tau^h$ can be estimated in the following way. Assume that we have found a steady solution on grid $m-1$ with cell-size $2h$. Then compute $\tau_{2h}^{4h}$ on grid $m-2$ by (4.22). From this, $\tau^{4h}$ follows through (4.29a). Next, we apply (4.29b) twice to find subsequently $\tau^{2h}$ and $\tau^h$.

For the interpolation (4.29b) we have to use the same limiting-averaging procedure (2.11) as for $u$, because the discretization error $\tau^h$ can be discontinuous. For a first-order Godunov scheme, applied to the discontinuous problem (2.3), $\tau^h$ is discontinuous at the sonic point and at the shock. Roe's scheme smooths the discontinuity at the sonic point, from one to two cells. The second-order scheme has a smooth $\tau^h = O(h^2)$ almost everywhere, except at the shock, where $\tau^h$ is discontinuous and has a number of $O(h)$ spikes.

Once $\tau^h$ has been estimated, in either of the ways sketched above, we can test convergence by

$$\|\tau^h\| \leq \epsilon \|\tau^h\|. \tag{4.30}$$

For smooth problems, the $L_1$-, $L_2$-, or $L_\infty$-norms will be comparable. A local comparison, denoted by $L_{loc}$, will generally require smaller residuals. A natural choice is $\epsilon = 1$, although a smaller value may be necessary if $\tau_h^{2h}$ is computed from the unsteady solution.

A safe way to determine convergence is: test (4.30) for the $L_1$-norm, with $\epsilon = 1$, check if the $L_1$-norm of the residual has dropped by a factor $(\frac{1}{2})^{p+1}$, and test if the $L_\infty$-norm of the residual has dropped by a factor $\frac{1}{4}$. The motivation for this triple test lies in the properties of the discontinuous solution. The $L_1$-norm is fairly insensitive to the local behaviour at the shock for a first-order scheme, and can be accurate even if the steady state has not been fully reached. For a second-order scheme, however, the local $O(h)$-spikes in $\tau^h$ may increase the global $L_1$-norm, especially if the solution has not converged yet. In that case testing the drop in the residual is a safeguard. The $L_\infty$-norm measures the convergence near the shock. After grid-refinement and local relaxation, the initial residual around the shock may still be relatively large, so considering only the drop in the $L_\infty$-norm of the residual may result in a premature stop. The combination of the three tests gives a satisfactory performance (§5.2).

The error $E^h$ in the converged solution $\overline{u}^h$ can be estimated in a similar way as $\tau^h$:

$$E^h = (\tfrac{1}{2})^p I_{2h}^h(E^{2h}), \quad E^{2h} = \tfrac{1}{1-(\frac{1}{2})^p} E_h^{2h}, \quad E_h^{2h} = \overline{u}^{2h} - I_h^{2h}(\overline{u}^h). \tag{4.31}$$

A first-order Godunov scheme causes $E^h$ to be discontinuous at the sonic point, and Roe's scheme again smears out this discontinuity, but only slightly. For our problem, the error is almost continuous at the shock, apart form an $O(h)$ spike. The second-order Godunov or Roe scheme has $E^h = O(h^2)$, except at the shock, where a discontinuity and one or more spikes occur. These spikes are of $O(h^2)$ for the present problem, which has a practically flat solution on both sides of and near the shock. In general they may become $O(h)$ in the worst case.

**4.7. Choice of the time-step.** So far, we have not specified the construction of a fixed $\beta$. Because the value of $\beta$ under consideration may correspond to the stability limit, this construction should be carried out with care. We use an explicit scheme with

$$\left(\frac{1}{\Delta t}\right)_k = a_k^*/\beta, \quad a_k^* = \max_{l=k-p,\ldots,k+p} \left(-\phi_{kl} \frac{\partial r_k}{\partial u_l}\right), \quad \phi_{kk} = 1, \quad \phi_{kl\neq k} = -1. \tag{4.32}$$

If the expression for the average convection speed $a_k^*$ happens to provide zero, we simply set it to $h$.

The above choice (4.32) breaks down at the sonic point if Godunov's scheme is used. This can be seen as follows. Consider the residual in cell $k$. Let the state $u_{k-1} < 0$, $u_{k+1} > 0$, and $u_{k-1} < u_k < u_{k+1}$. For positive $u_k$, the first-order Godunov scheme yields $r_k = s_k - \frac{1}{2}u_k^2$. For negative $u_k$ we have $r_k = s_k + \frac{1}{2}u_k^2$. If the residual is evaluated at a coarser grid $H$, then the fine-to-coarse defect correction $\tau_h^H$ may be thought to be absorbed in $s_k$. Equation (4.32) now yields $\Delta t = 1/|u_k|$ if $\beta = 1$, thus providing Newton's method for solving $r_k = 0$. However, if $s_k$ and $u_k$ have different signs, then $u_k$ has to change its sign before the solution $\overline{u}_k$ to $r_k(\overline{u}_k) = 0$

can be found (assuming that the conditions $u_{k-1} < u_k < u_{k+1}$, $u_{k-1} < 0$, $u_{k+1} > 0$, remain valid all the way toward the steady state). In that case, Newton's method becomes unreliable, as $u_k$ may become very small, so that $r_k$ hardly changes and $\Delta t$ becomes extremely large, thus causing extremely large changes in the solution. For this reason, we prefer to use Roe's scheme.

**4.8. The singularity at the shock.** In the discontinuous case, we expect two kinds of problems. First, the interpolation operator $I_h^{2h}$ (4.21), that computes an initial guess on grid $h$ from the steady solution on grid $2h$, will cause a local error of $O(1)$ at the shock. In smooth regions the error will be $O(h^p)$. Therefore, something special has to be done at the shock to reduce the $O(1)$-error to $O(h^p)$, in order to take full advantage of the multigrid scheme. One could use a more sophisticated kind of interpolation, but it is easier to use local relaxation, which we have to use anyhow, as will be seen below.

The second problem is the singularity at the shock in the discrete equations. *Even under ideal circumstances, the asymptotic convergence rate $\overline{\lambda}$ for a first-order scheme can at best be $\frac{1}{2}$, if there is a shock.* To assert this, assume that we have two grids, a fine grid $m$ with cell-size $h$, and a coarse $m-1$ with cell-size $2h$. Also assume that the coarse-grid problem is solved exactly, and that the residuals are very small everywhere, even at the shock. In that case the errors $v_k^h$ will be small, except at the shock, where $v_M^h$ can still be large. Without loss of generality we may assume the index $M$ of the cell that contains the singularity, to be even. The coarse-grid error, after restriction, is $v_{\frac{1}{2}M}^H = \frac{1}{2}(v_M^h + v_{M+1}^h) \simeq \frac{1}{2}v_M^h$. The exact solution of the coarse grid is prolongated back to the fine grid, resulting in

$$\begin{aligned} \tilde{v}_M^h &= v_M^h - \tfrac{1}{2}v_M^h = \tfrac{1}{2}v_M^h, \\ \tilde{v}_{M+1}^h &= v_{M+1}^h - \tfrac{1}{2}v_M^h = -\tfrac{1}{2}v_M^h. \end{aligned} \tag{4.33}$$

If the new $\tilde{u}_M^h$ still obeys

$$\tilde{u}_{M-1}^h > \tilde{u}_M^h > \tilde{u}_{M+1}^h, \quad \text{with } \tilde{u}_{M-1}^h > 0,\ \tilde{u}_{M+1}^h < 0, \tag{4.34}$$

then only $\tilde{u}_{M+1}^h$ will result in fairly large residuals at $M$ and $M+1$. An ideal relaxation scheme such as CRB with $\beta = 1$, will first bring $\tilde{v}_{M+1}^h$ down to practically zero, causing the residuals at $M$ and $M+1$ to vanish. The error $\tilde{v}_M^h = \frac{1}{2}v_M^h$ will be unaffected. Thus the asymptotic convergence rate $\overline{\lambda} = \frac{1}{2}$ in this case. In general, we will have $\overline{\lambda} \geq \frac{1}{2}$.

There remains an open question: how can the coarse-grid problem be solved under the above assumptions? The residual on the coarse grid $m-1$, after restriction, is small, so how can $\tilde{v}_{M/2}^H$ be found? Moreover, the coarse-grid equations will be plagued by the same singularity. To resolve this issue, we have to consider a sequence of coarser grids. The coarsest grid with $N = 2$ will notice a deviation from the conservation condition (2.14), even if the residuals are zero, and make the appropriate correction. This correction is prolongated to the next fine grid ($N = 4$). If many multigrid cycles on $N = 4$ are made, the error will finally vanish on this grid, with a damping rate that at best is $\frac{1}{2}$. By induction we conclude that in this way the exact solution on grid $m-1$ can be found, as long as $\gamma$ is sufficiently large.

If a relaxation is scheme is used that is not ideal, and if smaller values for $\gamma$ are used, we may end up with a situation where the error at the singularity creates large residuals around the shock after the coarsest ($N = 2$) grid has been visited. In that case, we may not have convergence at all. We therefore need a special subroutine to remove the residuals around the the shock, and at the same time find the proper solution at the singularity. In view of (4.33), we propose to use *local relaxation* (cf. [2]) by a Switched Evolution/Relaxation Method (SER), with *local conservation* imposed as an extra condition. Let the set $\mathcal{L}$ denote the $L$ cells where this local relaxation is carried out. Here $L$ is generally much smaller than the total number of cells $N$. Because the

information for conservation is obtained form the coarser grid, $\mathcal{L}$ is chosen to cover a number of coarse-grid cells. This implies that $L$ is even, and that the first element of $\mathcal{L}$ corresponds to an even index $k$ on the fine grid.

The SER scheme is given by

$$\sum_{m=1}^{L}\left[\frac{1}{\Delta t}-\frac{\partial r_n}{\partial u_m}\right](\Delta_t u)_m = r_n, \quad m,\, n \in \mathcal{L}. \tag{4.35a}$$

For small time-steps, this scheme is practically explicit, hence time-accurate, whereas for large time-steps Newton's method is obtained. The choice

$$\frac{1}{\Delta t} = \max_{n\in\mathcal{L}}(|r_n|/a_n^*). \tag{4.35b}$$

makes (4.35a) into a SER scheme. Similar definitions for systems of equations can be found in [9,10,11,16]. For $\Delta t \to \infty$, the system (4.35a) becomes singular at the shock ($\partial r_n/\partial u_M = 0$), so the corresponding equation is replaced by the requirement of local conservation (even for small time-steps):

$$\sum_{m=1}^{L}(\Delta_t u)_m = 0, \quad \text{if } n = M, \quad m, M \in \mathcal{L}. \tag{4.35c}$$

In the present test problem, we choose $L = 4$. The set $\mathcal{L}$ is determined by finding the cell $k_M$ where the residual has its maximum absolute value. For $L = 4$, the first element of $\mathcal{L}$ corresponds to the largest index $k$, that is even and smaller than $k_M$. For these cells, the linear system (4.35) is set up and solved. The solution is updated, and the new residuals in $\mathcal{L}$ and the two neighbouring cells is computed. This process is repeated until a maximum number of steps has been reached, or until condition (4.30) is satisfied, or until the damping rate of $\|r^h\|$ in $\mathcal{L}$ becomes practically 1. For the latter, we use the $L_\infty$-norm. The entire routine may be repeated a number of times. Because $L \ll N$, in general, the cost of applying this routine is low compared to a full relaxation sweep. This routine is used after the interpolation of the coarse-grid steady state to the fine grid (4.21). It is also applied once directly after prolongation, on every grid.

**4.9. The sonic point.** The linear analysis based on a constant convection speed $a$ is not valid at the sonic point. A different approach is required to find the damping rates around this point. We will consider the Point-Jacobi scheme for a first-order-accurate solution as an example.

Let the sequence of cells $(2k, 2k+1, 2k+2, 2k+3)$ contain the sonic point. Renumber them as $(0, 1, 2, 3)$. The steady state $\overline{u}_k$ is written as $a_k$, and the error $v_k = a_k - u_k$ is assumed to be small with respect to $a_k$. A local expansion of $a_k$ can be made around $a_2$:

$$a_k = a_2 + (k-2)ha_2' + O(h^2), \quad \text{with } a_2' > 0. \tag{4.36}$$

On the coarse grid, we denote the various quantities by capital letters rather than using superscripts $h$ and $H$. Let $A_0 = \frac{1}{2}(a_0 + a_1) < 0$ and $A_1 = \frac{1}{2}(a_2 + a_3) > 0$. On the fine grid there are 2 cases, with a different position of the sonic point. In case 1, we let $a_2 < 0, a_3 > 0$, in case 2, we have $a_1 < 0, a_2 > 0$. It is convenient to write

$$\text{case 1}: \quad a_2 = -\tfrac{1}{2}\alpha h a_2', \tag{4.37a}$$

$$\text{case 2}: \quad a_2 = \tfrac{3}{2}\alpha h a_2'. \tag{4.37b}$$

Note that in §3.2 we neglected terms of $O(h)$. This can not be done at the sonic point, because $a_2 = O(h)$.

The linearized residuals can be found from the fully nonlinear equations by neglecting terms of $O(v_k^2)$. For instance:

$$\left.\begin{aligned} r_0 &= s_0 - \tfrac{1}{2}(u_1^2 - u_0^2) \\ s_0 &= \tfrac{1}{2}(a_1^2 - a_0^2) \\ u_k &= a_k - v_k \end{aligned}\right\} \quad \Rightarrow r_0 \simeq a_1 v_1 - a_0 v_0. \tag{4.38}$$

A relaxation step with Point-Jacobi lets $\tilde{v} = v - \beta r_k / a_k^*$, where $a_k^*$ follows from (4.32). For instance, $a_0^* = \max(-a_0, -a_1) = -a_0$. In this way we find in case 1:

$$S^{(1)} = I - \beta \begin{pmatrix} 1 & -\frac{2+\alpha}{4+\alpha} & 0 & 0 \\ 0 & 1 & -\frac{\alpha}{2+\alpha} & 0 \\ 0 & 0 & 1 & -\frac{\alpha}{2+\alpha} \\ 0 & 0 & -\frac{2-\alpha}{4-\alpha} & 1 \end{pmatrix}, \tag{4.39a}$$

and in case 2:

$$S^{(2)} = I - \beta \begin{pmatrix} 1 & \frac{3\alpha-2}{4-3\alpha} & 0 & 0 \\ 0 & 1 & \frac{3\alpha-2}{4-3\alpha} & 0 \\ 0 & \frac{-3\alpha}{2+3\alpha} & 1 & 0 \\ 0 & 0 & \frac{-3\alpha}{2+3\alpha} & 1 \end{pmatrix}. \tag{4.39b}$$

Here $S$ works on the vector $(v_0, v_1, v_2, v_3)^T$. The exact solution of the coarse-grid equations yields, in case 1:

$$\begin{aligned} \tilde{V}_0 &= [(5-\alpha)(4+\alpha)v_0 - 2\alpha(1-\alpha)v_2 + (2-\alpha)(3+\alpha)v_3]/16, \\ \tilde{V}_1 &= [(1-\alpha)(4+\alpha)v_0 + 2\alpha(3+\alpha)v_2 + (2-\alpha)(7+\alpha)v_3]/16. \end{aligned} \tag{4.40a}$$

In the other case:

$$\begin{aligned} \tilde{V}_0 &= [(4-3\alpha)(5+3\alpha)v_0 + 3\alpha(1+3\alpha)v_1 - (2-3\alpha)(1+3\alpha)v_2 + 3(1-\alpha)(2+3\alpha)v_3]/16, \\ \tilde{V}_1 &= [(4-3\alpha)(1+3\alpha)v_0 - 9\alpha(1-\alpha)v_1 + 3(1-\alpha)(2-3\alpha)v_2 + (7-3\alpha)(2+3\alpha)v_3]/16. \end{aligned} \tag{4.40b}$$

From this solution the new errors on the fine grid can be found, e.g., $\tilde{v}_0 = v_0 - \tilde{V}_0$. In this way we can compute the CGC operator K. The spectral radius $\overline{\lambda}$ of $K.S$ depends on $(\alpha)$. For $\beta = \frac{1}{2}$ and $\alpha \in [0, 1]$, we have

$$\text{case 1}: \quad 0.318 \leq \overline{\lambda} \leq 0.359, \tag{4.41a}$$

$$\text{case 2}: \quad \overline{\lambda} = 0.5\,. \tag{4.41b}$$

Recall that we found $\overline{\lambda} = 0$ in the case of constant $a$. Thus, the asymptotic convergence rate will be dominated by the slower convergence at the sonic point.

For the other relaxation schemes we may expect a similar slow-down, or even instability. One could consider a special treatment of the sonic point, e.g., by using additional local relaxation. In practice, only convergence down to the truncation error is desired. The local relaxation that is applied for a number of times right after grid-refinement will not only take care of the region around the shock, but also of the region around the sonic point, since the truncation error is large over there, and therefore also the initial residuals. This may be sufficient to avoid a slow-down of the overall convergence during the first few cycles.

**4.10. Summary.** We have analyzed the performance of a few relaxation schemes in a multigrid context. Standard multigrid analysis can be used for the smooth regions of the flow. Convection, which is the physical property of the differential equation in smooth regions, allows for the

construction of ideal relaxation schemes. Here the multigrid technique works very well. On the other hand, there are problems at positions where the convection speed changes sign.

The upwind differencing causes the loss of one discrete equation in the cell that contains the shock. This reflect the physical property of shocks to absorb incoming signals, but at the same time makes the steady-state problem ill-posed. The result is slower convergence, as argued in §4.8. The correct steady state at the shock can be recovered by using local conservation. The required information can be obtained from the coarser grid. The local relaxation (4.35) handles this situation.

At the shock we lose a discrete equation. At the sonic point, we effectively gain one, as is obvious from (4.39). This causes the local damping rate to deviate from its overall value. If the local damping is larger than the overall, one may consider a special treatment of the sonic point. Because there is an additional discrete equation, one could find the local steady state directly by considering two cells simultaneously (but only in the first-order case). This implies, again, local relaxation. Alternatively, the relaxation parameter $\beta$ could be optimized separately for the sonic point. However, we have decided to do nothing special at the sonic point during the multigrid correction cycle, as we expect that the local relaxation applied after grid-refinement will be sufficient to find the steady state within truncation error.

## 5. Numerical examples

**5.1. Asymptotic convergence rates.** The above algorithm has been coded for the smooth and discontinuous examples of Eqs.(2.2) and (2.3), respectively. For the smooth case, we expect a good agreement with the estimated damping rates. In the discontinuous case, local relaxation should take care of the singularity near the shock. The sonic point may still cause deviations from the predicted damping rates for constant convection speed.

The asymptotic convergence rate $\overline{\lambda}$ holds for a large number of points $N$ and an exact CGC-operator. For finite $N$, there will be an $O(h)$ deviation. To make this small, we have made runs for a grid with $N = 512$ cells. For the first-order CGC, we use the CRB scheme, with $\beta = 1$, $\nu_1 = 0$, $\nu_2 = 1$, and $\gamma = 2$. This covers the first-order-accurate solutions [$p = 1$], and the second-order-accurate ones that are obtained with a first-order CGC [$p = (2, 1)$]. For the second-order CGC, we use the same relaxation scheme on the grid $m-1$ as on the finest grid $m$, with the same $\nu_1$ and $\nu_2$ as on the finest grid. On grid $m - 1$, we let $\gamma = 3$ to make sure that the coarse-grid problem is solved almost exactly. For the subsequent coarser grids $m - 2, m - 3, \ldots$, the amount of work would become rather large with $\gamma = 3$, so we use the same first-order CGC as above, but now with respect to grid $m - 1$ rather than to the finest grid $m$.

Local relaxation is only applied in the discontinuous case. After grid-refinement, at most 8 sweeps are made for the first-order-accurate solution, and at most 12 for the second-order-accurate one. In both cases, the search for the largest residual is carried out at most 4 times, so for the first-order-accurate solution the local relaxation is repeated at the same 4 points for at most 2 times, for the second-order-accurate solution at most 3 times. During the multigrid correction cycle, we only carry out local relaxation once on 4 cells.

The evaluation of the numerical damping rate $\overline{\lambda}$ involves some arbitrariness. The initial values of the state quantities $u_k$ are taken from the solution on the coarser grid. Thus, the higher frequencies will dominate the error. During the first few cycles, the damping rate is mainly determined by the behaviour of these high frequencies. After this phase, the convergence rate becomes more or less constant, until round-off errors start to dominate. The numerical damping rates have to be estimated from the part of the convergence history between the initial phase and the noise-level.

For the results shown in Table 3, 10 multigrid cycles on the finest grid were carried out, from which the damping rate per cycle was estimated. For the larger values of $\overline{\lambda}$, this usually involved all but the first cycle.

It turns out that the actual result is practically the same for the $L_1$-, $L_2$-, and $L_\infty$-norm of either the error $v^h$ or the residual $r^h$, although the $L_\infty$-norm is less constant from step to step. The results in Table 3 are based on the $L_1$-norm, and are given for both the error $v^h$ and the residual $r^h$.

The linear analysis predicts identical results for $(\nu_1, \nu_2) = (1, 0)$ and $(\nu_1, \nu_2) = (0, 1)$. The differences that occur in Table 3 give an indication of the accuracy of the estimated damping rates, as do the differences between the results for $v^h$ and $r^h$.

In most of the cases, there is a good agreement between analysis and experiment. The sonic point, occurring in the discontinuous case causes slower convergence for PJ, $p = 1$, for MS and RB, if $p = 1$ and $\nu_1 = \nu_2 = 1$, and for SRB and CSRB if $p = 1$. The SRB and CSRB schemes are mildly unstable at the sonic point for second-order-accurate solutions [$p = (2, 1)$ or $p = 2$], although not in all cases. This instability starts to dominate after the rest of the solution has converged toward the steady state.

**5.2. Fast convergence.** The above results show that our linear analysis is valid. It can be used to evaluate the quality of the several relaxation schemes. For practical purposes, these asymptotic convergence rates are less important. In a FMG-context, the initial guess is obtained from the steady solution on the coarser grid. In that case, the damping of the first multigrid cycle can be much better than predicted by the asymptotic damping rate. The initial error must be damped by a factor $(\frac{1}{2})^{1+p}$ to become comparable to the truncation error. For some relaxation schemes, this is already accomplished before the asymptotic regime is entered.

Consider the computation of a first-order-accurate steady state. For most of the examples presented in Table 3, the asymptotic damping rates $\overline{\lambda} \leq 0.25$, so one F-cycle per grid can be expected to suffice. Table 4a shows results obtained in this way. We use the optimal values for the relaxation parameter $\beta$, as in Table 3, but, contrary to §5.1, the same relaxation scheme is used on every grid. The quantity

$$\delta_q^h \equiv \|u^h - \overline{u}^h\|_q / \|\overline{u}^h - u_c^h\|_q. \tag{5.1}$$

Here the numerical steady state $\overline{u}^h$ has a zero residual, whereas $u_c^h$ is the cell-averaged stationary solution of the differential equation. The total amount of work $w$ is computed by counting the number of cells in which the residual is evaluated, and dividing by the number of cells on the finest grid. For the smooth solution, these values are consistent with (4.26). The total amount of work $w$ for the discontinuous case is higher, because of the local relaxation sweep on 4 cells after prolongation. Because F-cycles involve many visits to the coarser grids, the relative amount of work spent on local relaxation is somewhat large.

Table 4a shows that cycles with $(\nu_1, \nu_2) = (0, 1)$ are preferable above those with $(\nu_1, \nu_2) = (1, 0)$. The smaller amount of work for the former in the discontinuous case is due to the fact that the local relaxation routine is applied in the neighbourhood of the residual of largest size, hence requires the residual to be known everywhere. When $\nu_2 = 0$, the residual is computed on the entire current grid, although it is modified in only $4 + 2$ cells.

The Point-Jacobi scheme with $(\nu_1, \nu_2) = (0, 1)$ is clearly the most cost-effective choice. The Semi Red-Black scheme is slightly faster, but obviously less robust. For the latter, one cycle is not always sufficient.

For a second-order-accurate solution the use of a first-order CGC appears more attractive than a second-order CGC, because the second-order-accurate residual is substantially more expensive than a first-order-accurate. Table 4b shows results obtained with a first-order CGC, using a fixed number of F-cycles on every currently finest grid. The same relaxation scheme is used on the fine and coarser grids, but with a different optimal parameter $\beta$ for the finest and the coarser grids. The number of cycles $\kappa$ is based on the estimated asymptotic convergence rate $\overline{\lambda}$. For PJ, MS, and RB, we obtain convergence well below the truncation error. The SRB scheme, which

is unstable at the sonic point in some cases (§5.1), performs less satisfactorily. In some cases we need more cycles to obtain a converged solution, in others also W-cycles instead of F-cycles.

**5.3. Deferred Correction technique.**

In the previous paragraph, a first-order CGC was used to obtain second-order-accurate solutions. Instead of using first-order-accurate residuals only on the coarser grids, one may use them on the finest grid as well. In that case we compute a term

$$\sigma_k^h = r_k^h(p=2) - r_k^h(p=1) \tag{5.2}$$

at the begin of every multigrid correction cycle. The term is added to the first-order residual during relaxation and restriction. This technique is known as the deferred correction technique (cf. [3]). The computation of (5.2) involves some additional work, but this is compensated by the lower cost of the first-order scheme.

For the local relaxation after grid-refinement, as applied in the discontinuous case, we use the second-order-accurate residual. The quantities $\sigma_k^h$ are computed at the begin of every multigrid correction cycle, and kept fixed until the next cycle. Because it is not clear what the asymptotic convergence rate will be, we have used the stopping criterion (4.30) with $\epsilon = 1$, and with the additional requirement that the $L_1$-norm of the residual must drop by a factor $\frac{1}{8}$, and its $L_\infty$-norm by $\frac{1}{4}$.

Numerical results are shown in Table 4c. Again, PJ with $(\nu_1, \nu_2) = (0,1)$ seems to be the best choice. The SRB scheme does not convergence is some cases, as might have been expected by now.

**5.4. Tau-extrapolation.** In §4 it was discussed how to estimate the truncation error $\tau^h$. These estimates can actually be used to improve the accuracy of the solution. The technique is call $\tau$-extrapolation.

The simplest implementation estimates $\tau^{2h}$ from $\tau_h^{2h}$ according to (4.29a), and adds this instead of $\tau_h^{2h}$ to the coarse-grid residual (4.23). However, this introduces an inconsistency between the finest and coarser grids, which slows down convergence when the residual becomes comparable to the truncation error. Consistency can be recovered by adding the current estimate of $\tau^h$ to the fine-grid residual during relaxation. The initial $\tau^h$ at the beginning of the iterations on grid $h$, can be estimated from $\tau_{2h}^{4h}$, using (4.29). At the restriction from $h$ to $2h$ we compute $\tau_h^{2h}$ and modify the residual at grid $2h$ by means of $\tau^{2h}$. At the same time a new estimate of the fine-grid truncation error $\tau^h$ is obtained through (4.29b).

Table 5 shows the errors in the steady solutions obtained in this way. The first and second row give the results without $\tau$-extrapolation. Both the $L_1$- and $L_\infty$-norm of the error are given. These values are obtained by averaging $\|E^h\|/h^p$ from the grids with $N = 32$ to $N = 512$. The third and fourth row show the effect of $\tau$-extrapolation: the order of the solution is increased by 1. An exception is the discontinuous case. As remarked in §4, $\tau^h$ is discontinuous at the shock and at the sonic point if $p = 1$, and has $O(h)$-spikes around the shock if $p = 2$. Consequently, the $\tau$-extrapolation loses its accuracy at these isolated spots. This shows up in the $L_\infty$-norms for the discontinuous case.

## 6. Conclusions

The analysis and experiments show that the standard multigrid techniques can be applied to a nonlinear hyperbolic conservation law of the type studied here. In regions where the convection speed is well above, or below, zero, ideal damping rates [of $O(h)$] can be obtained. If the convection speed changes its sign, however, this ideal behaviour is lost. At the shock we have a singularity in the discrete equations. This is a result of dropping the time-accuracy. The singularity can be removed by augmenting the equations with Rankine-Hugoniot jump conditions,

which is equivalent to requiring local conservation as an additional constraint. Information about conservation is obtained from coarser grids, through a special kind of local relaxation. At the sonic point, the analysis is not applicable, but in most cases this is not a serious problem.

We have analyzed 3 schemes: Point-Jacobi, a Two-Stage scheme, and Red-Black relaxation. Point-Jacobi appears the simplest and most cost-effective, both for first-order and second-order accuracy. Its cheaper variant, Semi Red-Black, is theoretically appealing, but not very robust. Normal Red-Black relaxation loses its direction-free property when used in combination with the CGC operator. One either needs underrelaxation ($\beta = \frac{1}{2}$), or must take the direction of convection into account (Convective Red-Black).

The main mechanisms for smoothing are damping and convection. Damping causes smearing and dissipation of the error. Convection shifts errors around. It can profitably be used to make errors equal in neighbouring cells, which is ideal for a smoother. In the presence of a shock or a boundary, there is another mechanism to get rid of errors. In the neighbourhood of a shock, convection shifts errors toward the shock, where they are absorbed, whereas near a boundary the simply leave the computational domain. Thus, a boundary or shock will change the local the behaviour of the multigrid scheme. It may be that, on a relatively coarse grid, the schemes with underrelaxation ($\beta < 1$) are less efficient than those with $\beta = 1$, even if the latter are unstable. However, on much finer grids, this can no longer be true.

First-order-accurate steady states can be obtained in one F-cycle, independent of the number of cells in the computational domain. A second-order-accurate solution requires about 4 such cycles, using either a first-order CGC scheme, or the deferred correction technique.

First-order upwind differencing is a good starting point for the construction of efficient solvers. It directly reflects the physical behaviour of the differential equation and does not suffer from the spurious oscillatory phenomena that require the use of artificial viscosity in central-difference schemes. It is therefore easier to pinpoint, and interpret, the difficulties that may occur in actual applications. In addition, efficient relaxation methods are easier to construct for upwind-difference than for central-difference schemes.

The present results can be easily generalized to systems of equations in one dimension, specifically the Euler equations of gas-dynamics. Roe's scheme allows the use of characteristic equations without violating conservation. For each of these equations, the above results are valid. Even the convective variants can be generalized, as can the "time-step" (4.32).

It should be remarked that in one dimension we may just as well use tridiagonal solvers [9]. For two dimensional problems the use of the multigrid technique is more important. Unfortunately, analyzing relaxation schemes and the CGC operator is much harder, because the two-dimensional Euler equations of gas-dynamics are not simultaneously diagonalizable in both spatial dimensions. A scalar model equation of the form

$$u_t + au_x + bu_y = 0 \tag{6.1}$$

is not applicable (except when both the x- and y-components of the velocity are supersonic) and one needs to resort to systems of equations, which complicates the analysis.

## References


[1] G.D. van Albada, B. van Leer, and W.W. Roberts, *A Comparative Study of Computational Methods in Cosmic Gas Dynamics*, Astron. Astrophys. 108 (1982), pp. 76-84

[2] D. Bai and A. Brandt, *Local Mesh Refinement Multilevel Techniques*, SIAM J. Sci. Stat. Comput. (1986), in press.

[3] A. Brandt, *Guide to Multigrid Development*, Lecture Notes in Mathematics 960 (1981), pp. 220-312.

[4] W. Hackbusch, *Multi-grid Convergence Theory*, Lecture Notes in Mathematics 960 (1981), pp. 177-219.

[5] P.W. Hemker, S.P. Spekreijse, *Multiple grid and Osher's scheme for the efficient solution of the steady Euler equations*, CWI Report NM-R8507, to appear in Appl. Num. Math. (1986)
[6] A. Jameson, *Solution of the Euler Equations for Two-Dimensional Transonic Flow by a Multigrid Method*, Appl. Math. Comp. 13 (1983), pp. 327-356
[7] D.C. Jespersen, *Design and Implementation of a Multigrid Code for the Euler Equations*, Appl. Math. Comp. 13 (1983), pp. 357-374.
[8] B. Koren, *Euler flow solutions for a transonic windtunnel section*, CWI Report NM-R8601 (1986).
[9] W.A. Mulder and B. van Leer, *Experiments with Implicit Upwind Methods for the Euler Equations*, J. Comp. Phys. 59 (1985), pp. 232-246.
[10] W.A. Mulder, *Multigrid Relaxation for the Euler Equations*, J. Comp. Phys. 60 (1985), pp. 235-252.
[11] W.A. Mulder, *Computation of the Quasi-Steady Gas Flow in a Spiral Galaxy by Means of a Multigrid Method*, Astron. Astrophys. 156 (1986), pp. 354-380.
[12] P.L. Roe, *Approximate Riemann Solvers, Parameter vectors, and Difference Schemes*, J. Comp. Phys. 43 (1981), pp. 357-372.
[13] K. Stüben, U. Trottenberg, *Multigrid Methods: Fundamental Algorithms, Model Problem Analysis and Applications*, Lecture Notes in Mathematics 960 (1981), pp. 1-176.
[14] B. van Leer, *Towards the Ultimate Conservative Difference Scheme. IV. A New Approach to Numerical Convection*, J. Comp. Phys. 23 (1975), pp. 276-299.
[15] B. van Leer, *On the Relation between the Upwind-Differencing Schemes of Godunov, Enquist-Osher, and Roe*, SIAM J. Sci. Stat. Comput. 5 (1984), pp. 1-20.
[16] B. van Leer and W.A. Mulder, *Relaxation Methods for Hyperbolic Conservation Laws*, in Numerical Methods for the Euler Equations of Fluid Dynamics, eds. F. Angrand, A. Dervieux, J.A. Desideri, and R. Glowinski, SIAM, Philadelphia (1985), pp. 312-333.

| accuracy | first-order | | second-order | |
|---|---|---|---|---|
| scheme | $\beta$ | $\overline{\mu}$ | $\beta$ | $\overline{\mu}$ |
| PJ | $\frac{1}{2}$ | 0.707 | $(\frac{1}{5})$ | (0.949) |
| MS | $\frac{1}{3}$, 1 | 0.333 | 0.350, 0.592 | 0.645 |
| RB | 0.682 | 0.457 | 0.510 | 0.806 |

**Table 1.** *Choices of $\beta$ for which $\overline{\mu}$ is smallest. The results are given for one relaxation step ($\nu = 1$). Second-order PJ is unstable.*

| Point-Jacobi | | $\nu = 1$ | | $\nu = 2$ | |
|---|---|---|---|---|---|
| $p$ | $\beta$ | $\overline{\mu}$ | $\overline{\lambda}$ | $\overline{\mu}^2$ | $\overline{\lambda}$ |
| 1 | $\frac{1}{2}$ | 0.707* | 0 * | 0.5 * | 0.5 |
| | $\frac{1}{3}$ | 0.745 | 0.333 | 0.556 | 0.111* |
| 2, 1 | $\frac{1}{5}$ | 0.949* | 0.671* | 0.9 * | 0.654 |
| | 0.147 | 0.952 | 0.707 | 0.907 | 0.650* |
| 2 | $\frac{1}{5}$ | 0.949* | 0.717 | 0.9 * | 0.692 |
| | 0.145 | 0.953 | 0.711* | 0.908 | 0.685 |
| | 0.150 | 0.952 | 0.711 | 0.906 | 0.685* |

**Table 2a.** *Asymptotic multigrid convergence rates for Point-Jacobi relaxation. Optimal values are denoted by an asterisk. Second-order PJ is unstable. The notation $p = 2, 1$ means: $p = 2$ on the finest grid, $p = 1$ on the coarse.*

| Multi-Stage | | | $\nu = 1$ | | $\nu = 2$ | |
|---|---|---|---|---|---|---|
| $p$ | $\beta_1$ | $\beta_2$ | $\overline{\mu}$ | $\overline{\lambda}$ | $\overline{\mu}^2$ | $\overline{\lambda}$ |
| 1 | $\frac{1}{3}$ | 1 | 0.333* | 0.333 | 0.111* | 0.248 |
| | 0 | $\frac{1}{2}$ | 0.707 | 0 * | 0.5 | 0.5 |
| | −0.399 | 0.202 | 0.877 | 0.436 | 0.769 | 0.076* |
| 2, 1 | 0.350 | 0.592 | 0.645* | 0.677 | 0.417* | 0.761 |
| | 0.237 | 0.369 | 0.768 | 0.612* | 0.589 | 0.615 |
| | 0.283 | 0.281 | 0.763 | 0.757 | 0.582 | 0.573* |
| 2 | 0.350 | 0.592 | 0.645* | 0.645 | 0.417* | 0.761 |
| | 0.295 | 0.588 | 0.719 | 0.517* | 0.516 | 0.911 |
| | 0.280 | 0.448 | 0.714 | 0.605 | 0.510 | 0.366* |

**Table 2b.** *Asymptotic two-grid convergence rates for Two-Stage relaxation. For $\beta_1 = 0$ this scheme reduces to Point-Jacobi.*

| Red-Black | | $\nu = 1$ | | | $\nu = 2$ | | |
|---|---|---|---|---|---|---|---|
| $p$ | $\beta$ | $\overline{\mu}$ | $\overline{\lambda}(e,o)$ | $\overline{\lambda}(o,e)$ | $\overline{\mu}$ | $\overline{\lambda}(e,o)$ | $\overline{\lambda}(o,e)$ |
| 1 | 0.682 | 0.457* | 0.101 | 0.830 | 0.115 | 0.084 | 0.564 |
| | 0.704 | 0.459 | 0.088 | 0.904 | 0.094* | 0.079 | 0.582 |
| | 1 | 0.707 | 0 * | 2 | 0.707 | 0 * | 2 |
| | $\frac{1}{2}$ | 0.530 | 0.25 | 0.25 * | 0.283 | 0.063 | 0.442 |
| | 0.339 | 0.666 | 0.437 | 0.437 | 0.448 | 0.191 | 0.191* |
| 2,1 | 0.510 | 0.806* | 0.538 | 0.754 | 0.621 | 0.501 | 1.460 |
| | 0.769 | 0.933 | 0.455 | 2.507 | 0.385* | 0.405 | 1.207 |
| | 0.941 | 1.176 | 0.409* | 3.945 | 1.020 | 0.339 | 3.285 |
| | 0.907 | 1.118 | 0.414 | 3.648 | 0.798 | 0.332* | 2.330 |
| | 0.273 | 0.868 | 0.611 | 0.639* | 0.758 | 0.562 | 0.648 |
| | 0.185 | 0.908 | 0.663 | 0.663 | 0.826 | 0.596 | 0.627* |
| 2 | 0.510 | 0.806* | 0.552 | 0.676 | 0.621 | 0.421 | 1.460 |
| | 0.769 | 0.933 | 0.440 | 2.507 | 0.385* | 0.366 | 0.816 |
| | 0.928 | 1.153 | 0.386* | 3.829 | 0.929 | 0.302 | 2.901 |
| | 0.891 | 1.092 | 0.393 | 3.510 | 0.707 | 0.295* | 1.918 |
| | 0.405 | 0.821 | 0.596 | 0.636* | 0.679 | 0.473 | 1.006 |
| | 0.288 | 0.862 | 0.641 | 0.652 | 0.748 | 0.547 | 0.592* |

**Table 2c.** *Asymptotic multigrid convergence rates for Red-Black relaxation. The value of $\overline{\lambda}$ depends on the order in which the relaxation is carried out: $(e,o)$ means that first the even and then the odd points are relaxed ($k = 0, 1, \ldots, N-1$). For $(o,e)$ this order is reversed. All values are computed for $a > 0$. If $a < 0$ then the values $\overline{\lambda}(e,o)$ and $\overline{\lambda}(o,e)$ should be interchanged. The above optimal values of $\overline{\lambda}$ for the ordering $(o,e)$ are also optimal if both $a > 0$ and $a < 0$ occur.*

| Semi Red-Black | | $\nu = 1$ | $\nu = 2$ |
|---|---|---|---|
| $p$ | $\beta$ | $\overline{\lambda}$ | $\overline{\lambda}$ |
| 1 | 1 | 0 * | 0 * |
| 2,1 | 1.216 | 0.458* | 0.958 |
| | 0.941 | 0.515 | 0.409* |
| 2 | 0.626 | 0.693* | 0.657 |
| | 0.586 | 0.693 | 0.656* |

**Table 2d.** *Asymptotic multigrid convergence rates for Semi Red-Black relaxation.*

| Point-Jacobi | | | | | smooth | | discontinuous | |
|---|---|---|---|---|---|---|---|---|
| $p$ | $\beta$ | $\nu_1$ | $\nu_2$ | $\bar{\lambda}$ | $\bar{\lambda}(v)$ | $\bar{\lambda}(r)$ | $\bar{\lambda}(v)$ | $\bar{\lambda}(r)$ |
| 1 | $\frac{1}{2}$ | 1 | 0 | 0 | 0.0067 | 0.0061 | 0.269 | 0.215 |
| | | 0 | 1 | | 0.0068 | 0.013 | 0.265 | 0.317 |
| | $\frac{1}{3}$ | 1 | 1 | 0.111 | 0.112 | 0.112 | 0.241 | 0.211 |
| 2,1 | 0.2 | 1 | 0 | 0.671 | 0.671 | 0.680 | 0.649 | 0.675 |
| | | 0 | 1 | | 0.672 | 0.680 | 0.653 | 0.676 |
| | 0.147 | 1 | 1 | 0.650 | 0.577 | 0.585 | 0.558 | 0.582 |
| 2 | 0.145 | 1 | 0 | 0.711 | 0.736 | 0.768 | 0.736 | 0.761 |
| | | 0 | 1 | | 0.740 | 0.768 | 0.739 | 0.762 |
| | 0.150 | 1 | 1 | 0.685 | 0.592 | 0.578 | 0.588 | 0.575 |

**Table 3a.** *Asymptotic multigrid convergence rates for Point-Jacobi relaxation, as estimated from the numerical experiments on a grid with 512 cells.*

| Multi-Stage | | | | | | smooth | | discontinuous | |
|---|---|---|---|---|---|---|---|---|---|
| $p$ | $\beta_1$ | $\beta_2$ | $\nu_1$ | $\nu_2$ | $\bar{\lambda}$ | $\bar{\lambda}(v)$ | $\bar{\lambda}(r)$ | $\bar{\lambda}(v)$ | $\bar{\lambda}(r)$ |
| 1 | $\frac{1}{3}$ | 1 | 1 | 0 | 0.333 | 0.328 | 0.332 | 0.284 | 0.330 |
| | | | 0 | 1 | | 0.333 | 0.332 | 0.283 | 0.329 |
| | −0.399 | 0.202 | 1 | 1 | 0.076 | 0.076 | 0.076 | 0.285 | 0.258 |
| 2,1 | 0.237 | 0.369 | 1 | 0 | 0.612 | 0.623 | 0.633 | 0.604 | 0.629 |
| | | | 0 | 1 | | 0.626 | 0.633 | 0.609 | 0.630 |
| | 0.283 | 0.281 | 1 | 1 | 0.573 | 0.560 | 0.568 | 0.543 | 0.566 |
| 2 | 0.295 | 0.588 | 1 | 0 | 0.517 | 0.514 | 0.503 | 0.511 | 0.502 |
| | | | 0 | 1 | | 0.509 | 0.503 | 0.508 | 0.501 |
| | 0.280 | 0.448 | 1 | 1 | 0.366 | 0.371 | 0.365 | 0.371 | 0.366 |

**Table 3b.** *Asymptotic multigrid convergence rates for Multi-Stage relaxation.*

| Red-Black | | | | | | smooth | | discontinuous | |
|---|---|---|---|---|---|---|---|---|---|
| $p$ | $\beta$ | *order* | $\nu_1$ | $\nu_2$ | $\overline{\lambda}$ | $\overline{\lambda}\,(v)$ | $\overline{\lambda}\,(r)$ | $\overline{\lambda}\,(v)$ | $\overline{\lambda}\,(r)$ |
| 1 | $\frac{1}{2}$ | $(e,o)$ | 1 | 0 | 0.25 | 0.249 | 0.251 | 0.284 | 0.254 |
| | | | 0 | 1 | | 0.251 | 0.251 | 0.281 | 0.261 |
| | | $(o,e)$ | 1 | 0 | | 0.249 | 0.251 | 0.266 | 0.256 |
| | | | 0 | 1 | | 0.251 | 0.251 | 0.277 | 0.264 |
| | 0.339 | $(e,o)$ | 1 | 1 | 0.191 | 0.192 | 0.191 | 0.226 | 0.201 |
| | | $(o,e)$ | 1 | 1 | | 0.192 | 0.191 | 0.226 | 0.205 |
| 2,1 | 0.273 | $(e,o)$ | 1 | 0 | 0.639 | 0.601 | 0.611 | 0.582 | 0.611 |
| | | | 0 | 1 | | 0.604 | 0.611 | 0.587 | 0.606 |
| | | $(o,e)$ | 1 | 0 | | 0.602 | 0.611 | 0.582 | 0.610 |
| | | | 0 | 1 | | 0.604 | 0.611 | 0.586 | 0.607 |
| | 0.185 | $(e,o)$ | 1 | 1 | 0.627 | 0.519 | 0.527 | 0.501 | 0.525 |
| | | $(o,e)$ | 1 | 1 | | 0.519 | 0.527 | 0.501 | 0.526 |
| 2 | 0.405 | $(e,o)$ | 1 | 0 | 0.636 | 0.496 | 0.483 | 0.491 | 0.480 |
| | | | 0 | 1 | | 0.465 | 0.463 | 0.463 | 0.463 |
| | | $(o,e)$ | 1 | 0 | | 0.502 | 0.495 | 0.491 | 0.480 |
| | | | 0 | 1 | | 0.461 | 0.465 | 0.463 | 0.465 |
| | 0.288 | $(e,o)$ | 1 | 1 | 0.592 | 0.400 | 0.400 | 0.405 | 0.408 |
| | | $(o,e)$ | 1 | 1 | | 0.402 | 0.412 | 0.410 | 0.417 |

**Table 3c.** *Asymptotic multigrid convergence rates for Red-Black relaxation.*

| Convective Red-Black | | | | | smooth | | discontinuous | |
|---|---|---|---|---|---|---|---|---|
| $p$ | $\beta$ | $\nu_1$ | $\nu_2$ | $\overline{\lambda}$ | $\overline{\lambda}\,(v)$ | $\overline{\lambda}\,(r)$ | $\overline{\lambda}\,(v)$ | $\overline{\lambda}\,(r)$ |
| 1 | 1 | 1 | 0 | 0 | 0.0030 | 0.0029 | 0.042 | 0.031 |
| | | 0 | 1 | | 0.0026 | 0.0029 | 0.049 | 0.062 |
| | | 1 | 1 | | 0.0030 | 0.0033 | 0.018 | 0.030 |
| 2,1 | 0.941 | 1 | 0 | 0.409 | 0.147 | 0.154 | 0.221 | 0.280 |
| | | 0 | 1 | | 0.128 | 0.151 | 0.234 | 0.303 |
| | 0.907 | 1 | 1 | 0.332 | 0.125 | 0.157 | 0.209 | 0.287 |
| 2 | 0.928 | 1 | 0 | 0.386 | 0.245 | 0.242 | 0.274 | 0.290 |
| | | 0 | 1 | | 0.173 | 0.198 | 0.261 | 0.297 |
| | 0.891 | 1 | 1 | 0.295 | 0.146 | 0.169 | 0.238 | 0.296 |

**Table 3d.** *Asymptotic multigrid convergence rates for Convective Red-Black relaxation.*

| Semi Red-Black | | | | | | smooth | | discontinuous | |
|---|---|---|---|---|---|---|---|---|---|
| $p$ | $\beta$ | *order* | $\nu_1$ | $\nu_2$ | $\overline{\lambda}$ | $\overline{\lambda}(v)$ | $\overline{\lambda}(r)$ | $\overline{\lambda}(v)$ | $\overline{\lambda}(r)$ |
| 1 | 1 | $(e,o)$ | 1 | 0 | 0 | 0.0063 | 0.0056 | 0.312 | 0.219 |
| | | | 0 | 1 | | 0.0074 | 0.0063 | 0.348 | 0.312 |
| | | $(o,e)$ | 1 | 0 | | 0.0034 | 0.0032 | 0.303 | 0.208 |
| | | | 0 | 1 | | 0.0030 | 0.0036 | 0.358 | 0.312 |
| | | $(e,o)$ | 1 | 1 | | 0.0022 | 0.0030 | 0.322 | 0.311 |
| | | $(o,e)$ | 1 | 1 | | 0.0030 | 0.0033 | 0.317 | 0.294 |
| 2,1 | 1.216 | $(e,o)$ | 1 | 0 | 0.458 | 0.172 | 0.173 | 1.068 | 0.956 |
| | | | 0 | 1 | | 0.173 | 0.199 | 0.916 | 0.941 |
| | | $(o,e)$ | 1 | 0 | | 0.172 | 0.195 | 0.976 | 0.906 |
| | | | 0 | 1 | | 0.117 | 0.175 | 1.106 | 1.117 |
| | 0.941 | $(e,o)$ | 1 | 1 | 0.409 | 0.158 | 0.163 | 0.680 | 0.588 |
| | | $(o,e)$ | 1 | 1 | | 0.135 | 0.164 | 0.788 | 0.678 |
| 2 | 0.626 | $(e,o)$ | 1 | 0 | 0.693 | 0.543 | 0.543 | 0.532 | 0.534 |
| | | | 0 | 1 | | 0.509 | 0.502 | 0.511 | 0.499 |
| | | $(o,e)$ | 1 | 0 | | 0.516 | 0.499 | 0.532 | 0.532 |
| | | | 0 | 1 | | 0.508 | 0.500 | 0.511 | 0.501 |
| | 0.586 | $(e,o)$ | 1 | 1 | 0.656 | 0.408 | 0.399 | 0.397 | 0.406 |
| | | $(o,e)$ | 1 | 1 | | 0.332 | 0.352 | 0.385 | 0.406 |

**Table 3e.** *Asymptotic multigrid convergence rates for Semi Red-Black relaxation.*

| Convective Semi Red-Black | | | | | smooth | | discontinuous | |
|---|---|---|---|---|---|---|---|---|
| $p$ | $\beta$ | $\nu_1$ | $\nu_2$ | $\overline{\lambda}$ | $\overline{\lambda}(v)$ | $\overline{\lambda}(r)$ | $\overline{\lambda}(v)$ | $\overline{\lambda}(r)$ |
| 1 | 1 | 1 | 0 | 0 | 0.0034 | 0.0032 | 0.369 | 0.242 |
| | | 0 | 1 | | 0.0074 | 0.0063 | 0.269 | 0.292 |
| | | 1 | 1 | | 0.0022 | 0.0030 | 0.273 | 0.288 |
| 2,1 | 1.216 | 1 | 0 | 0.458 | 0.172 | 0.195 | 0.334 | 0.332 |
| | | 0 | 1 | | 0.173 | 0.199 | 0.920 | 0.914 |
| | 0.941 | 1 | 1 | 0.409 | 0.158 | 0.163 | 1.200 | 1.053 |
| 2 | 0.626 | 1 | 0 | 0.693 | 0.516 | 0.499 | 0.515 | 0.501 |
| | | 0 | 1 | | 0.509 | 0.502 | 0.508 | 0.498 |
| | 0.586 | 1 | 1 | 0.656 | 0.408 | 0.399 | 1.054 | 0.632 |

**Table 3f.** *Asymptotic multigrid convergence rates for Convective Semi Red-Black relaxation.*

| | | | smooth | | | discontinuous | | |
|---|---|---|---|---|---|---|---|---|
| scheme | $\nu_1$ | $\nu_2$ | $\delta_1^h$ | $\delta_\infty^h$ | $w$ | $\delta_1^h$ | $\delta_\infty^h$ | $w$ |
| PJ | 1 | 0 | 0.69 | 2.8 | 15.3 | 0.064 | 0.37 | 23.4 |
| | 0 | 1 | 0.066 | 0.11 | 15.3 | 0.022 | 2.2 | 18.5 |
| | 1 | 1 | 0.058 | 0.14 | 22.8 | 0.012 | 0.39 | 26.2 |
| MS | 1 | 0 | 0.12 | 0.35 | 22.8 | 0.025 | 0.29 | 31.0 |
| | 0 | 1 | 0.005 | 0.009 | 22.8 | 0.012 | 0.12 | 26.1 |
| | 1 | 1 | 0.26 | 0.54 | 38.0 | 0.021 | 1.0 | 41.2 |
| RB | 1 | 0 | 0.039 | 0.16 | 22.8 | 0.038 | 0.61 | 31.0 |
| $(e,o)$ | 0 | 1 | 0.011 | 0.019 | 22.8 | 0.019 | 0.15 | 26.0 |
| | 1 | 1 | 0.012 | 0.026 | 38.0 | 0.009 | 0.27 | 41.2 |
| RB | 1 | 0 | 0.86 | 2.3 | 22.8 | 0.045 | 1.4 | 31.0 |
| $(o,e)$ | 0 | 1 | 0.094 | 0.17 | 22.8 | 0.016 | 1.0 | 26.1 |
| | 1 | 1 | 0.041 | 0.10 | 38.0 | 0.012 | 0.33 | 41.3 |
| CRB | 1 | 0 | 0.004 | 0.008 | 22.8 | 0.010 | 0.069 | 30.9 |
| | 0 | 1 | 0.002 | 0.002 | 22.8 | 0.022 | 0.25 | 26.1 |
| | 1 | 1 | 0.003 | 0.005 | 38.0 | 0.007 | 0.049 | 41.2 |
| SRB | 1 | 0 | 18 | 79 | 15.3 | 0.57 | 11 | 23.3 |
| $(e,o)$ | 0 | 1 | 0.002 | 0.003 | 15.3 | 0.136 | 11 | 18.6 |
| | 1 | 1 | 0.004 | 0.009 | 22.8 | 0.058 | 6.3 | 26.1 |
| SRB | 1 | 0 | 0.003 | 0.012 | 15.3 | 0.38 | 3.3 | 23.3 |
| $(o,e)$ | 0 | 1 | 2.3 | 4.2 | 15.3 | 0.33 | 17 | 18.6 |
| | 1 | 1 | 0.004 | 0.011 | 22.8 | 0.074 | 5.9 | 26.1 |
| CSRB | 1 | 0 | 0.003 | 0.012 | 15.3 | 0.032 | 3.1 | 23.3 |
| | 0 | 1 | 0.002 | 0.003 | 15.3 | 0.068 | 10 | 18.4 |
| | 1 | 1 | 0.004 | 0.009 | 22.8 | 0.076 | 5.0 | 26.1 |

**Table 4a.** *Convergence levels and amount of work for a first-order-accurate steady state on a grid with 512 cells, when one F-cycle is carried out on every grid ($\kappa = 1$, $\gamma = 2$).*

| | | | | smooth | | | discontinuous | | |
|---|---|---|---|---|---|---|---|---|---|
| scheme | $\nu_1$ | $\nu_2$ | $\kappa$ | $\delta_1^h$ | $\delta_\infty^h$ | $w$ | $\delta_1^h$ | $\delta_\infty^h$ | $w$ |
| PJ | 1 | 0 | 6 | 0.016 | 0.038 | 92 | 0.008 | 0.015 | 125 |
| | 0 | 1 | 6 | 0.024 | 0.037 | 92 | 0.010 | 0.008 | 106 |
| | 1 | 1 | 5 | 0.014 | 0.029 | 114 | 0.007 | 0.036 | 127 |
| MS | 1 | 0 | 5 | 0.018 | 0.047 | 114 | 0.009 | 0.010 | 143 |
| | 0 | 1 | 5 | 0.024 | 0.042 | 114 | 0.009 | 0.032 | 127 |
| | 1 | 1 | 4 | 0.060 | 0.12 | 152 | 0.010 | 0.008 | 162 |
| RB | 1 | 0 | 5 | 0.016 | 0.026 | 114 | 0.008 | 0.038 | 142 |
| $(e,o)$ | 0 | 1 | 5 | 0.019 | 0.032 | 114 | 0.011 | 0.145 | 127 |
| | 1 | 1 | 5 | 0.008 | 0.018 | 190 | 0.004 | 0.003 | 202 |
| RB | 1 | 0 | 5 | 0.016 | 0.048 | 114 | 0.009 | 0.089 | 143 |
| $(o,e)$ | 0 | 1 | 5 | 0.024 | 0.040 | 114 | 0.011 | 0.14 | 127 |
| | 1 | 1 | 5 | 0.010 | 0.020 | 190 | 0.004 | 0.013 | 202 |
| CRB | 1 | 0 | 3 | 0.0003 | 0.002 | 68 | 0.0002 | 0.001 | 87 |
| | 0 | 1 | 3 | 0.0003 | 0.001 | 68 | 0.0004 | 0.003 | 77 |
| | 1 | 1 | 2 | 0.014 | 0.21 | 76 | 0.001 | 0.006 | 82 |
| SRB | 1 | 0 | 3 | 3.7 | 25 | 46 | 1.5 | 20 | 64 |
| $(e,o)$ | 0 | 1 | 3 | 0.004 | 0.010 | 46 | 1.7 | 48 | 54 |
| | 1 | 1 | 3 | 0.005 | 0.011 | 68 | 0.001 | 0.016 | 77 |
| SRB | 1 | 0 | 3 | 0.0001 | 0.002 | 46 | 2.4 | 35 | 64 |
| $(o,e)$ | 0 | 1 | 3 | — | — | 46 | — | — | 54 |
| | 1 | 1 | 3 | 0.0003 | 0.001 | 68 | 0.001 | 0.027 | 77 |
| CSRB | 1 | 0 | 3 | 0.0001 | 0.002 | 46 | 0.004 | 0.15 | 64 |
| | 0 | 1 | 3 | 0.0004 | 0.010 | 46 | 5.4 | 194 | 54 |
| | 1 | 1 | 3 | 0.0005 | 0.011 | 68 | 0.35 | 7.0 | 77 |

**Table 4b.** *Convergence levels and amount of work for a second-order-accurate steady state on a grid with* 512 *cells, when* $\kappa$ *F-cycles are carried out on every grid. A first-order CGC is used* $(p = 2, 1)$.

| | | | smooth | | | discontinuous | | |
|---|---|---|---|---|---|---|---|---|
| scheme | $\nu_1$ | $\nu_2$ | $\delta_1^h$ | $\delta_\infty^h$ | $w$ | $\delta_1^h$ | $\delta_\infty^h$ | $w$ |
| PJ | 1 | 0 | 0.013 | 0.041 | 96 | 0.023 | 0.087 | 114 |
| | 0 | 1 | 0.20 | 0.59 | 57 | 0.070 | 2.1 | 92 |
| | 1 | 1 | 0.011 | 0.040 | 83 | 0.11 | 2.7 | 97 |
| MS | 1 | 0 | 0.020 | 0.063 | 114 | 0.16 | 1.4 | 116 |
| | 0 | 1 | 0.011 | 0.028 | 111 | 0.084 | 0.59 | 112 |
| | 1 | 1 | 0.023 | 0.060 | 236 | 0.082 | 0.96 | 186 |
| RB | 1 | 0 | 0.016 | 0.066 | 92 | 0.034 | 0.17 | 112 |
| $(e,o)$ | 0 | 1 | 0.012 | 0.038 | 89 | 0.064 | 0.64 | 100 |
| | 1 | 1 | 0.010 | 0.034 | 128 | 0.051 | 0.48 | 118 |
| RB | 1 | 0 | 0.017 | 0.040 | 183 | 0.039 | 0.27 | 119 |
| $(o,e)$ | 0 | 1 | 0.021 | 0.048 | 116 | 0.089 | 2.1 | 99 |
| | 1 | 1 | 0.017 | 0.076 | 134 | 0.055 | 1.1 | 136 |
| CRB | 1 | 0 | 0.025 | 0.077 | 45 | 0.021 | 0.33 | 67 |
| | 0 | 1 | 0.029 | 0.063 | 42 | 0.18 | 7.6 | 110 |
| | 1 | 1 | 0.024 | 0.077 | 65 | 0.14 | 1.7 | 113 |
| SRB | 1 | 0 | — | — | — | — | — | — |
| $(e,o)$ | 0 | 1 | 0.062 | 0.24 | 31 | — | — | — |
| | 1 | 1 | 0.035 | 0.16 | 42 | 0.030 | 0.31 | 65 |
| SRB | 1 | 0 | 0.010 | 0.036 | 45 | — | — | — |
| $(o,e)$ | 0 | 1 | — | — | — | — | — | — |
| | 1 | 1 | 0.013 | 0.037 | 57 | 0.043 | 0.29 | 62 |
| CSRB | 1 | 0 | 0.010 | 0.036 | 45 | 0.21 | 8.2 | 61 |
| | 0 | 1 | 0.062 | 0.24 | 31 | 0.37 | 15 | 92 |
| | 1 | 1 | 0.035 | 0.16 | 42 | 0.28 | 5.0 | 62 |

**Table 4c.** *Convergence levels and amount of work for a second-order-accurate steady state on a grid with 512 cells, when the deferred correction technique is used.*

| | smooth | | discontinuous | |
|---|---|---|---|---|
| $p$ | $\|E^h\|_1$ | $\|E^h\|_\infty$ | $\|E^h\|_1$ | $\|E^h\|_\infty$ |
| 1 | $2.0\,h$ | $3.1\,h$ | $0.92\,h$ | $1.4\ \ h$ |
| 2 | $2.1\,h^2$ | $3.6\,h^2$ | $0.49\,h^2$ | $1.5\ \ h^2$ |
| $1 \rightarrow 2$ | $8.2\,h^2$ | $15\ \ h^2$ | $10\ \ h^2$ | $0.78\,h$ |
| $2 \rightarrow 3$ | $49\ \ h^3$ | $67\ \ h^3$ | $15\ \ h^3$ | $4.7\ \ h^2$ |

**Table 5.** *Solution errors without and with $\tau$-extrapolation.*

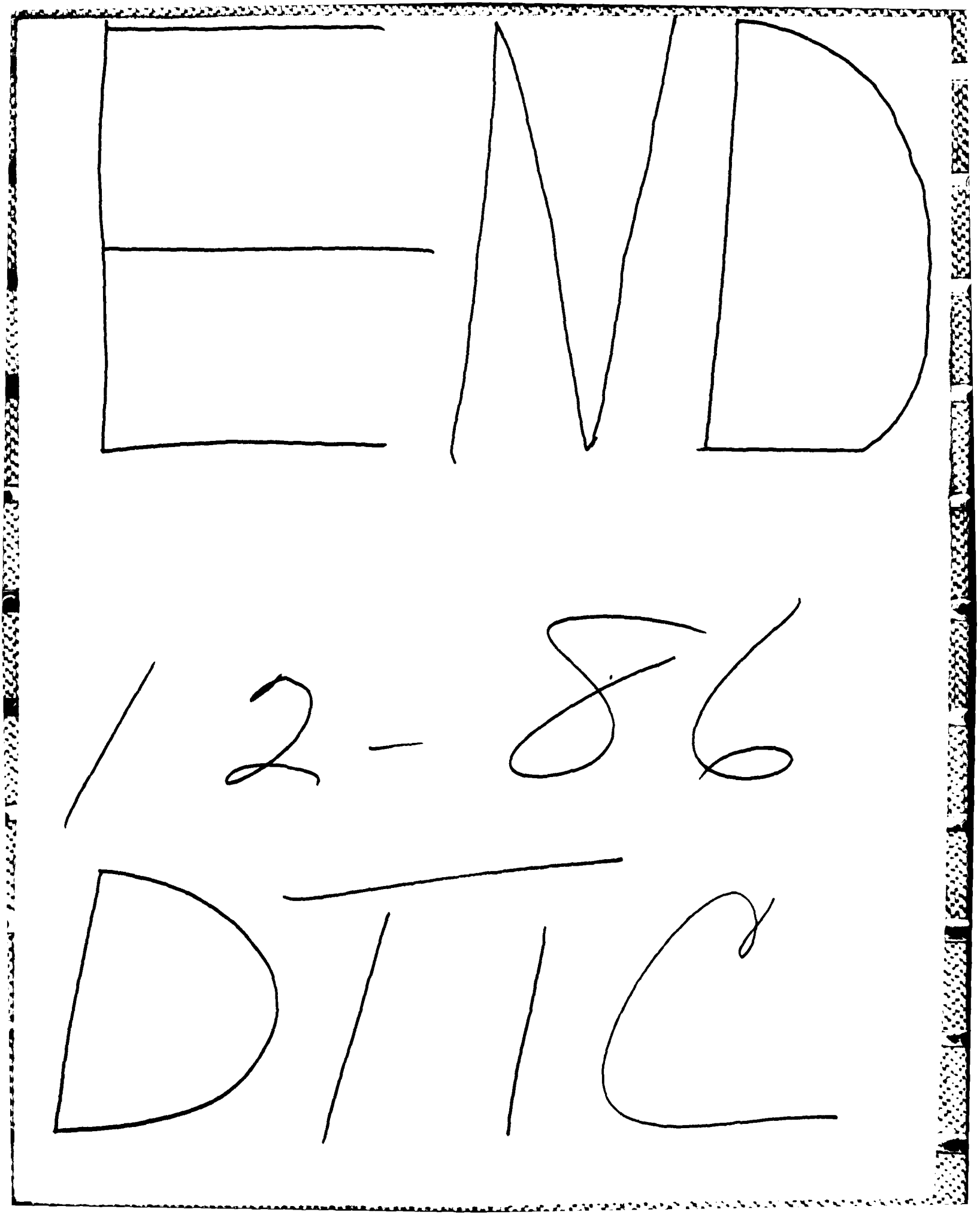
FMD
12-86
DTIC